Mechanical impact on the head has an antihypertensive effect

Authors:

Shuhei Murase[1,2,14], Naoyoshi Sakitani[1,14], Takahiro Maekawa[1], Daisuke Yoshino[3], Ayumu Konno[4], Hirokazu Hirai[4], Taku Saito[2], Sakae Tanaka[2], Keisuke Shinohara[5], Takuya Kishi[6], Yuki Yoshikawa[7], Takamasa Sakai[7], Makoto Ayaori[8], Hirohiko Inanami[9], Koji Tomiyasu[10], Toru Ogata[1,11], Atsushi Takashima[12], Masahiro Shinohara[1], Motoshi Nagao[1] and Yasuhiro Sawada[1,13]*

Affiliations:

[1]Department of Rehabilitation for Motor Functions, National Rehabilitation Center for Persons with Disabilities, Tokorozawa, Japan. [2]Department of Orthopaedic Surgery, Graduate School of Medicine, The University of Tokyo, Tokyo, Japan. [3]Division of Advanced Applied Physics, Institute of Engineering, Tokyo University of Agriculture and Technology, Koganei, Japan. [4]Department of Neurophysiology & Neural Repair, Gunma University Graduate School of Medicine, Maebashi, Japan. [5]Department of Cardiovascular Medicine, Kyushu University Graduate School of Medical Sciences, Fukuoka, Japan. [6]Department of Cardiology, Graduate School of Medicine, International University of Health and Welfare, Okawa, Japan. [7]Department of Bioengineering, Graduate School of Engineering, The University of Tokyo, Tokyo, Japan.

[8]Tokorozawa Heart Center, Tokorozawa, Japan. [9]Inanami Spine & Joint Hospital/Iwai Orthopaedic Medical Hospital, Iwai Medical Foundation, Tokyo, Japan. [10]Department of Internal Medicine, [11]Center of Sports Science and Health Promotion, [12]Department of Assistive Technology, [13]Department of Clinical Research, National Rehabilitation Center for Persons with Disabilities, Tokorozawa, Japan.

[14]These authors contributed equally: Shuhei Murase, Naoyoshi Sakitani.

*Correspondence to Yasuhiro Sawada, Department of Clinical Research, National Rehabilitation Center for Persons with Disabilities, 4-1 Namiki, Tokorozawa, Saitama 359-8555, Japan, Tel: +81-4-2995-3100, Fax: +81-4-2995-0355, Email: ys454-ind@umin.ac.jp

Abstract

Nervous cell functions are known to be physiologically regulated by mechanical factors in the brain. However, it remains unclear whether mechanical interventions can modulate the pathophysiological processes underlying brain-related disorders and modify their consequences. Here we show that passive head motion of hypertensive rats, which reproduces mechanical accelerations generated at their heads during treadmill running at a moderate velocity, decreases the expression of angiotensin II type 1 receptor (AT1R) in astrocytes in their rostral ventrolateral medulla (RVLM). This decrease results in lowering their blood

pressure. Passive head motion generates interstitial fluid movement that is estimated to exert shear stress with average magnitude of a few Pa on cells in rats' brainstem. Fluid shear stress of a relevant magnitude decreases AT1R expression in cultured astrocytes, but not in neuronal cells. Furthermore, in hypertensive rats, inhibition of movement of interstitial fluid by its gelation with reactive polyethylene glycol injected into the RVLM eliminates the ability of passive head motion to decrease their blood pressure and AT1R expression in RVLM astrocytes. Consistent with these results from animal experiments, vertically oscillating chair riding of hypertensive adult humans, which reproduces mechanical accelerations generated at their heads during light jogging or fast walking, lowers their blood pressure. Our findings indicate that moderate mechanical impact on the head has an antihypertensive effect by modulating the function of RVLM astrocytes through interstitial fluid shear stress. We anticipate mechanical regulation to underlie a variety of positive effects of physical exercise on human health, particularly those related to brain functions.

Introduction

Hypertension, which is a major cause of stroke and cardiovascular diseases, is the biggest risk factor for death worldwide[1]. Whereas numerous antihypertensive drugs have been developed and used clinically, physical exercise is known to be effective for the treatment and prevention of essential hypertension[2,3], which comprises the majority (>90%) of human hypertension[4]. Although

long-term regulation of blood pressure (BP) has been recognized to be largely dependent on sodium excretion adjusting systems, which mainly involve kidney functions[5], elevated activity of the sympathetic nervous system also importantly contributes to the development of hypertension[6-8]. Rostral ventrolateral medulla (RVLM), which is located in the brainstem, plays a critical role in determining the basal activity of the sympathetic nervous system, and its functional integrity is essential for the maintenance of basal vasomotor tone and regulation of BP[6,9]. Angiotensin II (Ang II) is the major bioactive peptide of the renin-angiotensin system (RAS), and is known to regulate BP as well as other biological processes such as cell growth/apoptosis/migration, inflammation, and fibrosis[10]. The biological effects of Ang II are mediated by its interaction with two distinct high-affinity G protein-coupled receptors, Ang II type 1 receptor (AT1R) and type 2 receptor. Of these receptors, AT1R is responsible for most of the known physiological and pathophysiological processes related to Ang II. Whereas RAS is involved in the functional regulation of various "peripheral" organs and tissues such as kidney and vessels, it also regulates brain functions within the blood-brain barrier, including the control and maintenance of sympathetic nerve activity and cognitive ability[11]. In particular, the role of AT1R signaling in the RVLM in cardiovascular regulation has been extensively studied and demonstrated. For example, the pressor/depressor responses to Ang II and Ang II antagonists, injected into the RVLM have been reported to be enhanced in spontaneously hypertensive rats (SHRs)[12,13]. We have previously demonstrated that

75 treadmill running at moderate velocities alleviates the sympathetic nerve activity, involving
76 attenuation of AT1R signaling in the RVLM of stroke-prone spontaneously hypertensive rats
77 (SHRSPs)[14], a substrain of SHRs that exhibit severer hypertension as compared with SHRs[15].
78 However, the details about the changes in AT1R signaling in the RVLM of these hypertensive rats
79 have yet to be elucidated. It remains unclear what type(s) of cells (e.g., neurons or astrocytes) are
80 primarily responsible for the altered AT1R signaling in the RVLM of SHRs or SHRSPs.
81 Furthermore, the causal relationship between the increased AT1R signal activity in the RVLM and
82 high BP in SHRs or SHRSPs in their steady state (i.e., apart from their responses to
83 pharmacological interventions) is left unrevealed.

84 AT1R has also been shown to play a vital role in regulating a variety of physiological or
85 pathological processes, including cellular responses to mechanical perturbations[16,17]. For example,
86 mechanical stretching of cardiac myocytes activates AT1R signaling[18], and fluid shear stress (FSS)
87 of average 1.5 Pa lowers AT1R expression in human vein endothelial cells[19]. Although intervening
88 the Ang II-AT1R system through pharmacological approaches, such as administration of
89 angiotensin-converting enzyme inhibitor or selective AT1R blocker, has been established as an
90 effective therapeutic strategy for hypertension[20], mechano-responsive attenuation of AT1R signaling
91 has not been clinically utilized as an antihypertensive measure.

92 Many of physical workouts, particularly aerobic exercises, involve vertical body motions,

which generate mechanical impacts (accelerations) on the head at the time of foot contact with the ground (i.e., landing). The importance of mechanical loads is well established in the physiological regulation of bones, the stiffest organ that only allows tiny deformation[21]. Osteocytes, the mechanosensory cells embedded in bones[22], are assumed to undergo minimal deformations under physiological conditions. We have reported that FSS on osteocytes derived from interstitial fluid flow induced upon physical activity plays an important role in maintaining bone homeostasis[23]. Given that the brain is not a rigid organ, minimally deforming forces or stress distribution changes in the brain during exercise or even activity of daily living (e.g., walking) may produce beneficial effects. We have previously shown that in the prefrontal cortex (PFC) of rodents, moderate mechanical impact-induced FSS modulates serotonin signaling in the neurons in situ[24]. Based on these previous findings together with the distribution of interstitial fluid throughout the whole brain, we hypothesized that moderate mechanical impact on the head might have antihypertensive effects involving FSS-mediated modulation of AT1R signaling in the RVLM.

Results

Application of cyclical mechanical impact to the head by passive motion lowers the BP in SHRSPs. To determine the effects of a mechanical intervention of a moderate intensity on BP, we first sought to develop an experimental system that reproduces the impact exerted on the head

during rats' treadmill running at a modest velocity (20 m/minute), a typical experimental intervention to test the effects of physical exercise on rats[25,26]. In a recent study, we observed that treadmill running of rats (20 m/minute) generated 5-mm vertical oscillation of their heads with ~1.0 x *g* peak accelerations and 2-Hz frequency; therefore, we developed a "passive head motion" (PHM) system to produce 2-Hz 5-mm vertical oscillation exerting 1.0 x *g* acceleration peaks at the heads of rats[24]. In the current study, we examined the effects of mechanical impact on BP in SHRSPs, using the PHM system. Similar to the antihypertensive effect of treadmill running on SHRs or SHRSPs that we and others reported previously[14,25,27], application of PHM (30 minutes/day, 28 consecutive days; see Fig. 1a) significantly lowered their BP (Fig. 1b,c) as compared to their controls, whereas HR was not significantly affected by PHM (Fig. 1d). Anesthesia alone (daily 30 minutes) did not significantly alter the BP in SHRSPs (Extended Data Fig. 1a), indicating that the antihypertensive effect resulted specifically from PHM. The anti-cardiac hypertrophy effect of PHM on SHRSPs (Fig. 1e) as well as the lack of these PHM effects on control normotensive rats (Wistar-Kyoto: WKY) (Fig. 1b,c,e) were also consistent with previous reports describing treadmill running as an antihypertensive intervention for SHRs[27]. As was observed in our treadmill running experiments[14], PHM decreased 24-hour urinary norepinephrine excretion of SHRSPs (Fig. 1f). This suggests that PHM mitigates the sympathetic hyperactivity[28]. Collectively, these results support our hypothesis that cyclical moderate mechanical impact on the head has an

antihypertensive effect.

PHM down-regulates AT1R expression in RVLM astrocytes of SHRSPs. We then looked into the mechanism of how PHM alleviated the development of hypertension in SHRSPs. We previously reported that down-regulation of AT1R signaling in the RVLM is responsible for the treadmill running-induced sympathoinhibition in SHRSPs[14]. Given the mechanical regulation of AT1R expression in endothelial cells[19], we examined whether PHM modulated AT1R expression in RVLM neurons and astrocytes of SHRSPs. In our histochemical analysis, we defined neuronal nuclei (NeuN)-positive cells as neurons[29] and glial fibrillary acidic protein (GFAP)-positive cells as astrocytes[30]. PHM (30 minutes/day, 28 days) did not significantly change the relative population of AT1R-expressing neurons and astrocytes in the RVLM of WKY rats (Fig. 1g). In contrast, 4-week PHM significantly decreased the expression of AT1R in the astrocytes, but not in the neurons, of SHRSPs' RVLM (Fig. 1h). Notably, AT1R expression in the RVLM neurons was comparable between WKY rats and SHRSPs, either with and without PHM (Fig. 1i). In contrast, AT1R expression was significantly higher in the RVLM astrocytes of SHRSPs without PHM (Fig. 1j, column 3). PHM lowered the AT1R expression in the RVLM astrocytes of SHRSPs to the level equivalent to that of WKY rats (Fig. 1j, columns 1, 2, and 4). Taken together, AT1R expression in RVLM astrocytes appeared to be correlated with the antihypertensive effect of PHM on SHRSPs. In

147 line with this observation, 4-week treadmill running of SHRSPs also decreased the AT1R
148 expression in their RVLM astrocytes, but not neurons (Extended Data Fig. 1b−d).
149
150 **PHM alleviates the sensitivity of RVLM in SHRSPs to Ang II or Ang II antagonist.** We next
151 sought to examine whether the PHM-induced decrease in AT1R expression in the RVLM astrocytes
152 of SHRSPs (Fig. 1j, columns 3 and 4) was functionally relevant to the suppression of AT1R
153 signaling. To this end, we analyzed the pressor responses to Ang II injected into unilateral RVLM of
154 WKY rats and SHRSPs, either subjected to 4-week PHM or left sedentary under anesthesia (30
155 minutes/day, 28 days) (Fig. 2a). As we previously reported[14], SHRSPs without PHM exhibited
156 significantly greater pressor response to Ang II administered to RVLM than WKY rats (Fig. 2b,
157 compare between top and bottom of left panels; Fig. 2c, compare columns 1 and 3). Four-week
158 PHM ameliorated the pressor response to Ang II injected into the RVLM of SHRSPs, but not of
159 WKY rats (Fig. 2b, compare left and right; Fig. 2c, compare columns 1 vs. 2 and 3 vs. 4).
160 Furthermore, depressor responses to Ang II antagonist injected into unilateral RVLM[13] of WHY rats
161 and SHRSPs with and without 4-week PHM appeared to be approximate mirror images of the
162 pressor responses (Fig. 2d,e). These results support the functional relevance of the PHM-induced
163 decrease in AT1R expression in the RVLM astrocytes of SHRSPs (Fig. 1j).
164 To examine whether the increased AT1R expression in the RVLM astrocytes of SHRSPs was

associated with their development of hypertension, we manipulated AT1R signaling by introducing exogenous expression of AT1R-associated protein (AGTRAP), which interacts with AT1R and tempers Ang II-mediated signals by promoting AT1R internalization[31]. To this end, we used an adeno-associated virus (AAV)-mediated gene delivery system[32]. AAV serotype 9 (AAV9) vectors were injected locally to transduce RVLM cells (Fig. 3a and Extended Data Fig. 2a). To achieve astrocyte- and neuron-specific gene expression, we used AAV9 vectors that harbored mouse GFAP promoter (AAV-GFAP) and rat neuron-specific enolase (NSE) promoter (AAV-NSE), respectively (Fig. 3a). Because these vectors contained a region encoding GFP and 2A sequence of porcine teschovirus-1 (P2A; self-cleaving peptides[33]) (Fig. 3a), observation of green fluorescence allowed us to identify the cells in which transgene was expressed (Fig. 3b,c and Extended Data Fig. 2a−e). AAV-mediated expression of AGTRAP in astrocytes (Fig. 3b) but not in neurons (Fig. 3c) of bilateral RVLMs in SHRSPs significantly lowered the BP as compared with their control SHRSPs in which only GFP was virally expressed in RVLM astrocytes or neurons (Fig. 3d,e). Furthermore, AAV-mediated expression of AGTRAP in astrocytes, but not neurons, of SHRSPs' bilateral RVLMs decreased 24-hour urinary norepinephrine excretion (Fig. 3f). Injection of control AAV vector (GFAP-control or NSE-control) did not significantly affect the BP of SHRSPs (Extended Data Fig. 2f). These results support the importance of AT1R signal intensity in RVLM astrocytes for SHRSPs' development of hypertension and sympathetic hyperactivity, as well as the physiological relevance

of PHM-induced decrease in AT1R expression we observed in the RVLM astrocytes of SHRSPs (Fig. 1j).

PHM generates low-amplitude pressure waves and induces interstitial fluid movement in rat RVLM. We then sought to determine the physical effects that PHM produced in rat RVLM. To do so, we analyzed local pressure changes using a telemetry pressure sensor (Fig. 4a) as we described previously[24]. PHM generated pressure waves (changes) with ~1.2 mm Hg peak amplitude (Fig. 4b−d). Hydrostatic pressure of this magnitude (~1.6 cm H_2O) is unlikely to initiate mechano-responsive signaling in cells[34]. Postulating an analogy to osteocytes embedded in bones, the function of which is known to be modulated by interstitial fluid flow-derived shear stress[23], we have demonstrated that minimal stress distribution changes generate interstitial fluid flow in the brain, resulting in shear stress-mediated regulation of nervous cell functions[24].

To analyze the PHM-induced interstitial fluid movement in the RVLM, we injected an iodine-based contrast agent (Isovist®) into the RVLM of anesthetized rats, and tracked its distribution with sequential computed tomography (CT) (Fig. 4e) as we previously did to quantify the movement of intramuscular interstitial fluid[35]. We found that PHM significantly promoted Isovist spreading in the rostral-caudal and dorsal-ventral (*y*- and *z*-axes, Fig. 4f) directions (Fig. 4g,h). In contrast, PHM did not significantly affect the left-right spreading (*x*-axis, Fig. 4f) of Isovist (Fig. 4g,h). As we

observed in rat PFC[24], PHM induced interstitial fluid movement in the brainstem in defined directions, rather than in an isotropic manner. Our simulative calculation suggests that PHM subjected RVLM cells to interstitial fluid flow-derived shear stress with an average magnitude of 0.59−2.64 Pa (Supplementary Table 1). FSS of this magnitude is known to modify the physiological function of astrocytes[36], leading us to hypothesize that FSS derived from interstitial fluid movement (Fig. 4e−h) mediated the PHM-induced decrease in AT1R expression in RVLM astrocytes (Fig. 1j).

FSS on astrocytes decreases AT1R expression in vitro. To test this hypothesis, we conducted in vitro FSS experiments. Based on our simulation (Supplementary Table 1), we applied pulsatile FSS with an average magnitude of 0.7 Pa to cultured primary astrocytes, which were prepared from astrocyte-GFP mice[37] (Extended Data Fig. 3a), using a system we previously reported[23,24,35,38]. Quantitative polymerase chain reaction (qPCR) and immunostaining analyses revealed that FSS application (0.5 Hz, 30 minutes) significantly decreased AT1R expression in astrocytes for at least 24 hours (Fig. 5a−c). In contrast, FSS application to Neuro2A cells, which exhibit neuronal phenotypes and morphology[39,40], did not decrease AT1R expression (Extended Data Fig. 3b−d). Consistent with the decreasing effect of FSS on AT1R expression, the binding of fluorescently labeled Ang II to cultured astrocytes was significantly decreased by pre-exposure to 30-minute FSS (Fig. 5d,e). The duration (>24 hours) of FSS effects on AT1R expression in astrocytes (Fig. 5) poses

a possibility of cumulative effects of FSS applied repeatedly at 24-hour intervals. Therefore, these in vitro observations suggest that FSS-mediated persistent reduction of AT1R expression is involved in the effects of daily PHM application on BP (Fig. 1b,c) and AT1R expression in the RVLM astrocytes (Fig. 1j) in SHRSPs.

Hindrance of interstitial fluid movement by hydrogel introduction in RVLM eliminates the ability of PHM to decrease the AT1R expression in RVLM astrocytes and the BP in SHRSPs.

To examine whether interstitial fluid movement in the RVLM mediated the effects of PHM on BP and AT1R expression in RVLM astrocytes of SHRSPs, we modulated local interstitial fluid dynamics. Following the procedure we used to hinder the interstitial fluid movement in mouse PFC[24], we gelled interstitial fluid in situ and deprived its fluidity by microinjecting mutually reactive polyethylene glycol (PEG) gel-precursor (pre-gel) solutions to RVLM (Fig. 6a). Injected pre-gel solution spread over rat RVLM, and gelled the interstitial fluid in situ (Extended Data Fig. 4a).

Hydrogel introduction in bilateral RVLMs eliminated the ability of PHM to decrease BP (Fig. 6b, black and orange lines; Fig. 6c, columns 2 and 3), urinary norepinephrine excretion (Fig. 6d, columns 2 and 3), and AT1R expression in the RVLM astrocytes (Fig. 6e, bottom 2 rows; Fig. 6f, columns 2 and 3) in SHRSPs. In contrast, hydrogel introduction increased BP (Fig. 6b, blue and

orange lines; Fig. 6c, columns 1 and 3), norepinephrine excretion (Fig. 6d, columns 1 and 3), and AT1R expression in the RVLM astrocytes (Fig. 6e, top 2 rows; Fig. 6f, columns 1 and 3) of SHRSPs subjected to PHM. AT1R expression in the RVLM neurons of SHRSPs remained unaltered irrespective of the combination of PHM and hydrogel introduction (Fig. 6e,g). These results suggest that hydrogel introduction in the RVLM disrupts the mechanism mediating the PHM-induced decrease in BP, norepinephrine excretion, and AT1R expression in the RVLM astrocytes of SHRSPs.

We previously showed that gelation only inhibits the fluidity of the fluid but does not restrict the diffusion of small molecules inside the gel[24,41]. Consistently, hydrogel introduction did not apparently delay or attenuate the depressor response to Ang II antagonist injected to the RVLM (Extended Data Fig. 4b−d), indicating rapid solute diffusivity through the hydrogels. As was the case with mouse PFC[24], gelation by injecting PEG solution did not affect overall cell number or apoptosis in RVLM (Extended Data Fig. 4e,f), and survival or apoptosis of RVLM astrocytes (Extended Data Fig. 4g,h) and neurons (Extended Data Fig. 4i,j). Collectively, the loss of PHM effects by hydrogel introduction in bilateral RVLMs of SHRSPs (Fig. 6b−f) is likely to result from hydrogel-mediated alteration in interstitial fluid dynamics, rather than decreased cell viability caused by impaired nutrient supply or removal of metabolic wastes.

Vertically oscillating chair riding (VOCR) lowers BP in hypertensive adult humans. The results from our animal experiments reveal the antihypertensive effect of mechanical accelerations generated at the head during treadmill running at a moderate velocity. This prompted us to test whether mechanical impact on the head lowered BP in hypertensive humans. As we observed light jogging or fast walking (locomotion at the velocity of 7 km/hour) typically produce ~2 Hz vertical acceleration waves with an amplitude of ~1.0 x *g* at the person's head (Extended Data Fig. 5a, top), we constructed a chair that could vertically oscillate at the frequency of 2 Hz (Extended Data Fig. 5b) and produce ~1.0 x *g* acceleration waves at the head of the occupant (Extended Data Fig. 5a, bottom).

Given that previous reports regarding antihypertensive effects of aerobic exercise typically recommend ≥3−4 days per week (frequency) and ≥30 minutes per session or day (duration)[3], we set our regimen of VOCR as 3 days/week (Monday, Wednesday, and Friday unless needed to assign otherwise for particular reasons such as public holidays) and 30 minutes/day. Our study of protocol 1, in which we simply compared the subjects' BP and HR before and after 4-week (12 times) VOCR (Extended Data Fig. 5c), showed that VOCR decreased BP in hypertensive humans (Fig. 7a).

We then conducted a human study of protocol 2, in which we followed the changes in subjects' BP and HR more minutely (Extended Data Fig. 5d). Encouraged by the positive results from the

study of protocol 1, we adopted the same VOCR regimen as to its frequency (3 days/week) and duration (30 minutes/day). Participants were subjected to serial blood sampling to measure plasma catecholamines (epinephrine, norepinephrine, and dopamine) and renin activity, and serum aldosterone and C-reactive protein (CRP) before and after the intervention period (Extended Data Fig. 5d). To conduct the 2nd blood sampling on the next day of the last bout of VOCR, the intervention period was extended from 4 weeks (total 12 times, typically 26 days) to 4.5 weeks (total 14 times, 30−31 days) because blood sampling could not be done during weekends at our hospital. BP, both systolic and diastolic, and MAP immediately after the intervention period significantly decreased as compared with those immediately before the intervention period (Fig. 7b). Furthermore, we also observed an antihypertensive effect of VOCR when we defined "BP of the week" to reliably detect the trends by reducing the influences from interday BP variability (see Methods) (Fig. 7c and Extended Data Fig. 6a). Notably, the post-intervention follow-up showed that the BP-lowering effect apparently persisted for 4 weeks, but not 5 weeks, after the last bout of VOCR (Fig. 7c). Similar to our animal study, we did not observe significant changes in HR by the VOCR intervention (Fig. 7a−c). Significant differences were not detected in the blood levels of catecholamines, aldosterone, renin activity, and CRP between before and after the VOCR intervention (Extended Data Fig. 6b).

Collectively, our studies of protocols 1 and 2 suggest that VOCR, which reproduces

291 mechanical impact exerted on the head during light jogging or fast walking, has an antihypertensive
292 effect in hypertensive humans. Importantly, in none of 21 subjects (Supplementary Table 2),
293 apparent adverse events, including motion sickness and low back pain, were observed or manifested
294 in relation to the VOCR intervention.
295
296 **Discussion**
297 Essential hypertension is defined as high BP in which secondary causes including renovascular
298 disease, renal failure, pheochromocytoma, and primary aldosteronism are not present. It accounts
299 for >90% of human cases of hypertension, resulting from combinations of multiple genetic and
300 environmental factors[4]. Recently, brain (dys)function has been implicated in the pathogenesis of
301 essential hypertension; however, the details of their molecular link remain unclear[42]. Physical
302 exercise is proven to be effective as a therapeutic/preventative measure for essential hypertension[3].
303 Although the antihypertensive effect of physical exercise has been shown to involve normalization
304 of sympathetic hyperactivity in the brain[43], it is still unclear whether exercise directly modulates
305 brain function. In this study, PHM, which reproduced mechanical accelerations generated at the
306 head during treadmill running, allowed us to dissect bodily activity-derived physical effects.
307 Whereas AT1R signaling in both neurons and astrocytes of the RVLM have been reported to be
308 involved in regulating BP[44,45], we observed that AT1R expression in RVLM astrocytes was

309 increased in SHRSPs as compared to that in WKY rats (Fig. 1j). In contrast, AT1R expression in
310 RVLM neurons was comparable between WKY rats and SHRSPs (Fig. 1i), although AT1R
311 expression in RVLM neurons has been shown to play an important role in other animal model(s) of
312 hypertension[44]. Together with the decreases in BP and urinary epinephrine excretion of SHRSPs in
313 which RVLM astrocytes were transduced with AGTRAP gene (Fig. 3d−f), the intensity of AT1R
314 signaling in RVLM astrocytes appears to be critically involved in the pathogenesis of hypertension
315 and sympathetic hyperactivity in SHRSPs.

316 Four-week PHM decreased urinary norepinephrine excretion and AT1R expression in RVLM
317 astrocytes of SHRSPs to the levels almost equivalent to those of WKY rats (Fig. 1f,j). However,
318 PHM only partially alleviated the development of hypertension in SHRSPs to the extent similar to
319 the antihypertensive effects of treadmill running we and others previously reported[14,25] (Fig. 1b,c).
320 Therefore, it is evident that factors other than AT1R signaling in RVLM astrocytes contribute to the
321 pathogenesis of essential hypertension.

322 AT1R expression in cultured astrocytes decreased upon FSS application (Fig. 5a−c). This was
323 consistent with our findings that PHM and treadmill running decreased in AT1R expression in
324 RLVM astrocytes of SHRSPs (Fig. 1j and Extended Data Fig. 1d). However, the AT1R expression
325 level in RVLM astrocytes was low in WKY rats even without PHM (Fig. 1j), and this may raise a
326 concern regarding the physiological relevance of our in vitro FSS experiments using cultured

327 astrocytes. Yet, it has been reported that cultured astrocytes typically exhibit increased "reactivity",
328 and do not fully recapitulate physiological astrocytes in vivo[46]. We suggest that the FSS-induced
329 decrease in AT1R expression in cultured astrocytes we observed represents physiological functions
330 of astrocytes, despite that their increased basal AT1R expression may relate to unphysiological
331 aspects of two-dimensional culture on stiff substrates (culture plastics). Cells in static culture are
332 exposed to a complete absence of FSS, which may not be physiologically realized in vivo. Previous
333 reports describe increased extracellular fluid in brains of hypertensive humans[47] and altered
334 dynamics of intracerebral interstitial fluid of SHRs[48]. Aberrant regulation of RVLM astrocytes'
335 function that relates to altered interstitial fluid movement-derived FSS may underlie the
336 pathogenesis of essential hypertension.

337 PHM did not significantly alter the AT1R expression in SHRSPs' RVLM neurons (Fig. 1i), and
338 FSS did not decrease AT1R expression in cultured Neuro2A cells (Extended Data Fig. 3b−d). Yet,
339 we do not suspect that these results represent the absence of sensitivity of neurons to FSS or other
340 type(s) of mechanical stimulation, particularly because we observed PHM- and FSS-induced
341 internalization of 5-HT_{2A} receptor expressed in mouse PFC neurons and Neuro2A cells,
342 respectively[24]. Alternatively, we speculate that PHM and FSS may mitigate hyperexpression of
343 AT1R related to aforementioned pathological status of SHRSPs' RVLM astrocytes or
344 unphysiological nature of cultured astrocytes. In line with this notion, PHM did not significantly

affect the AT1R expression in RVLM astrocytes in normotensive WKY rats (Fig. 1j). Relevantly, we and others have reported mechanical loading (in vivo)- or FSS (in vitro)- induced alleviation of inflammatory processes[23,49], which can transcriptionally increase AT1R expression[50].

Whereas the amplitude of pressure waves that PHM generated in rat RVLM was tiny (Fig. 4b−d), the magnitude of interstitial fluid movement-derived shear stress in rat RVLM appeared comparable with that of FSS previously reported for vascular endothelium[51,52], interstitium of bone[21] and skeletal muscle[35] (Supplementary Table 1b). Consistent with the lack of strict cell specificity in many of cellular responses to mechanical forces[53], FSS-induced decrease in AT1R expression, which was reported in vascular cells[19], was also observed in cultured astrocytes. Taken together, we speculate that there may be common homeostasis-regulatory mechanisms at the cellular level that involve fluid flow-derived shear stress of ~0.5 to a few Pa.

Based on our hypothesis concerning the similarity in the pathogenesis of high BP between human essential hypertension and SHRSPs, we conducted human studies in which we intended to reproduce the mechanical impact on the head that lowered the BP in SHRSPs. Although the mechanism behind the apparent antihypertensive effect of VOCR remains to be determined, the significant role of interstitial fluid dynamics in the RVLM, which we demonstrated by our animal experiments, might be shared between humans and rats or other animals (Extended Data Fig. 7). Whereas plasma catecholamine levels were not significantly changed by the VOCR intervention

(Extended Data Fig. 6b), it is possible that urinary epinephrine measures collected over 24 hours in our rat PHM experiments (Fig. 1f, 3f, and 6d) enhanced our ability to capture the sympathetic nerve activity under ‘‘everyday-life’’ ambulatory conditions[54].

As the phrase “Exercise is Medicine” indicates, physical exercise is broadly useful to maintain human health. Many of aerobic exercises, including walking and running, involve impact-generating bodily actions creating sharp accelerations at the head upon foot contacting with the ground. Therefore, their beneficial effects as therapeutic/preventative procedures for a variety of brain function-related diseases and health disorders may rely at least partly on modest changes in mechanical stress distribution in the brain, which may prompt optimal FSS on intracerebral nervous cells. While we have recently demonstrated that brain function can be physiologically regulated by mechanical forces[24], alterations in interstitial fluid movement-derived shear stress may underlie the pathogenesis of various brain disorders, particularly those related to physical inactivity or aging.

Limitation of study. There are several limitations of this study. We were unable to test the response of primary neurons, which were prepared from mouse cerebral cortex or hippocampus, to FSS of relevant magnitudes (0.59−2.64 Pa, see Supplementary Table 1b) because of their easy detachment from the substrates by FSS. As an alternative of cultured neuronal cells, we tested Neuro2A cells, which stably adhered to the substrates through FSS of magnitudes up to ~1 Pa[24].

We did not comprehensively analyze the effects of PHM on brain functions, but focused on the

study of RVLM. PHM may modulate AT1R signaling in other brain regions that participate in the regulation of sympathetic nerve activity, including the anteroventral third ventricle, paraventricular nucleus of the hypothalamus, and nucleus tractus solitarii[6,9]. Nonetheless, elimination of PHM effects on BP and urinary norepinephrine excretion by hydrogel introduction in RVLM (Fig. 6b−d) supports the critical role for RVLM. Because hydrogel may exert yet unknown effects, experiments of hydrogel introduction may not entirely prove the contribution of interstitial fluid movement. For example, hydrogel introduction may alter the stiffness and elasticity of extracellular matrix, which are known to affect the neurological physiology, pathology, and development[55]. Although further studies are required to address these issues, our findings suggest that mechanical factors can be a therapeutic target within the blood-brain barrier, the accessibility to which of antihypertensive drugs appears variable and controversial[56].

Unlike the case of PHM in rats, VOCR of humans generates vertical accelerations at various body parts in addition to the head. Therefore, we cannot preclude the possibility that the antihypertensive effect of VOCR is mediated by mechanical regulation of tissues and organs other than the brain. Furthermore, our clinical studies of protocol 1 and 2 are based on a small number of subjects (Supplementary Table 2) with a fixed condition (frequency of 2 Hz, peak acceleration of ~1.0 x *g*, 30 minutes/day, 3 days/week, 12−14 rides), and need further analysis with a much larger sample size and varying conditions to determine optimal VOCR. Still, application of vertical

399 mechanical impacts with moderate magnitudes is expected to be highly safe with minimal
400 possibility of adverse effects, providing a novel therapeutic/preventative strategy for physical
401 disorders including those that are resistant to conventional treatments such as drug administration.
402 Notably, our approach utilizing mechanical interventions may bring considerable benefits to those
403 who cannot receive benefits from exercise because of physical disabilities.
404

405 **Data availability**

406 All data are included in this article and its supplementary information files. Raw data are available
407 from the corresponding author upon reasonable request.
408

409 **Acknowledgements**

410 We thank K. Nakanishi, K. Hamamoto, and N. Kume for their consistent support. This work was in
411 part supported by Intramural Research Fund from the Japanese Ministry of Health, Labour and
412 Welfare; Grants-in-Aid for Scientific Research from the Japan Society for the Promotion of Science
413 (15H01820, 15H04966, and 18H04088 to Y.S; 17H02127 and 18H03138 to T.O.; 19K06899 to
414 A.K.); MEXT-Supported Program for the Strategic Research Foundation at Private Universities,
415 2015−2019 from the Japanese Ministry of Education, Culture, Sports, Science and Technology
416 (S1511017 to Y.S. and T.O.); Brain Mapping by Integrated Neurotechnologies for Disease Studies

from the Japan Agency for Medical Research and Development (AMED Brain/MINDS, JP20dm0207057 to H.H.).

Author contributions

S.M. and N.S. conducted most of the experiments. Y.S. conceived the research, designed the study, and led the project with help from M.N. and M.S. T.K. provided technical advice for all the experiments involving measurement of cardiovascular parameters. S.M., N.S., T.K., M.S. and Y.S. wrote the manuscript. T.M. and A.T. contributed to the design and construction of the machine for PHM. D.Y. helped in vitro FSS experiments and carried out simulative calculation of in vivo FSS. T.S. and Y.Y. developed and provided the PEG hydrogel system. A.K. and H.H. prepared and provided AAV vectors. K.T., T.K., M.A., H.I., and T.O. contributed to the human studies. K.S., T.S., S.T. M.S., T.O., and M.N. provided technical, advisory and financial support.

Competing interests

The authors declare no competing interest. S.M., T.M., T.O., A.T., and Y.S. joined the application of a patent for the vertically oscillating chair, which has been awarded in Japan (JP6592834) and filed internationally (US16/616,935; EP18806753.2; CN201880033284.0; IN201927048891).

References

1. Lim, S.S., *et al.* A comparative risk assessment of burden of disease and injury attributable to 67 risk factors and risk factor clusters in 21 regions, 1990-2010: a systematic analysis for the Global Burden of Disease Study 2010. *Lancet* **380**, 2224-2260 (2012).
2. Hagberg, J.M., Park, J.J. & Brown, M.D. The role of exercise training in the treatment of hypertension: an update. *Sports Med* **30**, 193-206 (2000).
3. Pescatello, L.S., MacDonald, H.V., Lamberti, L. & Johnson, B.T. Exercise for hypertension: a prescription update integrating existing recommendations with emerging research. *Curr Hypertens Rep* **17**, 87 (2015).
4. Carretero, O.A. & Oparil, S. Essential hypertension. Part I: definition and etiology. *Circulation* **101**, 329-335 (2000).
5. Guyton, A.C. Abnormal renal function and autoregulation in essential hypertension. *Hypertension* **18**, III49-53 (1991).
6. Guyenet, P.G. The sympathetic control of blood pressure. *Nat Rev Neurosci* **7**, 335-346 (2006).
7. Grassi, G., Mark, A. & Esler, M. The sympathetic nervous system alterations in human hypertension. *Circ Res* **116**, 976-990 (2015).
8. Malpas, S.C. Sympathetic nervous system overactivity and its role in the development of cardiovascular disease. *Physiol Rev* **90**, 513-557 (2010).
9. Dampney, R.A. Functional organization of central pathways regulating the cardiovascular system. *Physiol Rev* **74**, 323-364 (1994).
10. Fyhrquist, F. & Saijonmaa, O. Renin-angiotensin system revisited. *J Intern Med* **264**, 224-236 (2008).
11. Forrester, S.J., *et al.* Angiotensin II signal transduction: an update on mechanisms of physiology and pathophysiology. *Physiol Rev* **98**, 1627-1738 (2018).
12. Ito, S., Komatsu, K., Tsukamoto, K., Kanmatsuse, K. & Sved, A.F. Ventrolateral medulla AT1 receptors support blood pressure in hypertensive rats. *Hypertension* **40**, 552-559 (2002).
13. Muratani, H., Ferrario, C.M. & Averill, D.B. Ventrolateral medulla in spontaneously hypertensive rats: role of angiotensin II. *Am J Physiol* **264**, R388-395 (1993).
14. Kishi, T., *et al.* Exercise training causes sympathoinhibition through antioxidant effect in the rostral ventrolateral medulla of hypertensive rats. *Clin Exp Hypertens* **34**, 278-283 (2012).
15. Nabika, T., Ohara, H., Kato, N. & Isomura, M. The stroke-prone spontaneously hypertensive rat: still a useful model for post-GWAS genetic studies? *Hypertens Res* **35**, 477-484 (2012).
16. Lu, X., *et al.* Effects of local mechanical stimulation on coronary artery endothelial function and angiotensin II type 1 receptor in pressure or flow-overload. *J Hypertens* **31**, 720-729 (2013).

17. Galie, P.A., Russell, M.W., Westfall, M.V. & Stegemann, J.P. Interstitial fluid flow and cyclic strain differentially regulate cardiac fibroblast activation via AT1R and TGF-β1. *Exp Cell Res* **318**, 75-84 (2012).
18. Zou, Y.*, et al.* Mechanical stress activates angiotensin II type 1 receptor without the involvement of angiotensin II. *Nat Cell Biol* **6**, 499-506 (2004).
19. Ramkhelawon, B.*, et al.* Shear stress regulates angiotensin type 1 receptor expression in endothelial cells. *Circ Res* **105**, 869-875 (2009).
20. Li, E.C., Heran, B.S. & Wright, J.M. Angiotensin converting enzyme (ACE) inhibitors versus angiotensin receptor blockers for primary hypertension. *Cochrane Database Syst Rev*, CD009096 (2014).
21. Weinbaum, S., Cowin, S.C. & Zeng, Y. A model for the excitation of osteocytes by mechanical loading-induced bone fluid shear stresses. *J Biomech* **27**, 339-360 (1994).
22. Tatsumi, S.*, et al.* Targeted ablation of osteocytes induces osteoporosis with defective mechanotransduction. *Cell Metab* **5**, 464-475 (2007).
23. Miyazaki, T.*, et al.* Mechanical regulation of bone homeostasis through p130Cas-mediated alleviation of NF-κB activity. *Sci Adv* **5**, eaau7802 (2019).
24. Ryu, Y.*, et al.* Mechanical regulation underlies effects of exercise on serotonin-induced signaling in the prefrontal cortex neurons. *iScience* **23**, 100874 (2020).
25. Minami, N.*, et al.* Effects of exercise and β-blocker on blood pressure and baroreflexes in spontaneously hypertensive rats. *Am J Hypertens* **16**, 966-972 (2003).
26. Kim, S.E.*, et al.* Treadmill exercise prevents aging-induced failure of memory through an increase in neurogenesis and suppression of apoptosis in rat hippocampus. *Exp Gerontol* **45**, 357-365 (2010).
27. Bertagnolli, M.*, et al.* Exercise training reduces sympathetic modulation on cardiovascular system and cardiac oxidative stress in spontaneously hypertensive rats. *Am J Hypertens* **21**, 1188-1193 (2008).
28. Chidsey, C.A., Braunwald, E. & Morrow, A.G. Catecholamine excretion and cardiacstores of norepinephrine in congestive heart failure. *Am J Med* **39**, 442-451 (1965).
29. Mullen, R.J., Buck, C.R. & Smith, A.M. NeuN, a neuronal specific nuclear protein in vertebrates. *Development* **116**, 201-211 (1992).
30. Freeman, M.R. Specification and morphogenesis of astrocytes. *Science* **330**, 774-778 (2010).
31. Tamura, K.*, et al.* The physiology and pathophysiology of a novel angiotensin receptor-binding protein ATRAP/Agtrap. *Curr Pharm Des* **19**, 3043-3048 (2013).
32. Huda, F.*, et al.* Distinct transduction profiles in the CNS via three injection routes of AAV9 and the application to generation of a neurodegenerative mouse model. *Mol Ther Methods Clin Dev* **1**, 14032 (2014).

33. Tang, X., *et al.* "Self-cleaving" 2A peptide from porcine teschovirus-1 mediates cleavage of dual fluorescent proteins in transgenic Eimeria tenella. *Vet Res* **47**, 68 (2016).
34. Tworkoski, E., Glucksberg, M.R. & Johnson, M. The effect of the rate of hydrostatic pressure depressurization on cells in culture. *PLoS One* **13**, e0189890 (2018).
35. Saitou, K., *et al.* Local cyclical compression modulates macrophage function in situ and alleviates immobilization-induced muscle atrophy. *Clin Sci (Lond)* **132**, 2147-2161 (2018).
36. Maneshi, M.M., *et al.* Mechanical stress activates NMDA receptors in the absence of agonists. *Sci Rep* **7**, 39610 (2017).
37. Gong, S., *et al.* A gene expression atlas of the central nervous system based on bacterial artificial chromosomes. *Nature* **425**, 917-925 (2003).
38. Yoshino, D., Sakamoto, N., Takahashi, K., Inoue, E. & Sato, M. Development of Novel Flow Chamber to Study Endothelial Cell Morphology: Effects of shear flow with uniform spatial gradient ondistribution of focal adhesion. *J Biomech Sci Eng* **8**, 233-243 (2013).
39. Goshima, Y., Ohsako, S. & Yamauchi, T. Overexpression of Ca^{2+}/calmodulin-dependent protein kinase II in Neuro2A and NG108-15 neuroblastoma cell lines promotes neurite outgrowth and growth cone motility. *J Neurosci* **13**, 559-567 (1993).
40. Yun, J., *et al.* Neuronal Per Arnt Sim (PAS) domain protein 4 (NPAS4) regulates neurite outgrowth and phosphorylation of synapsin I. *J Biol Chem* **288**, 2655-2664 (2013).
41. Fujiyabu, T., Toni, F., Li, X., Chung, U.I. & Sakai, T. Three cooperative diffusion coefficients describing dynamics of polymer gels. *Chem Commun (Camb)* **54**, 6784-6787 (2018).
42. Jennings, J.R., Muldoon, M.F. & Sved, A.F. Is the brain an early or late component of essential hypertension? *Am J Hypertens* (2020).
43. Joyner, M.J. & Green, D.J. Exercise protects the cardiovascular system: effects beyond traditional risk factors. *J Physiol* **587**, 5551-5558 (2009).
44. Jancovski, N., *et al.* Angiotensin type 1A receptor expression in C1 neurons of the rostral ventrolateral medulla contributes to the development of angiotensin-dependent hypertension. *Exp Physiol* **99**, 1597-1610 (2014).
45. Guo, F., *et al.* Astroglia are a possible cellular substrate of angiotensin(1-7) effects in the rostral ventrolateral medulla. *Cardiovasc Res* **87**, 578-584 (2010).
46. Liddelow, S.A. & Barres, B.A. Reactive astrocytes: production, function, and therapeutic potential. *Immunity* **46**, 957-967 (2017).
47. Maclullich, A.M., *et al.* Higher systolic blood pressure is associated with increased water diffusivity in normal-appearing white matter. *Stroke* **40**, 3869-3871 (2009).
48. Bedussi, B., *et al.* Enhanced interstitial fluid drainage in the hippocampus of spontaneously hypertensive rats. *Sci Rep* **7**, 744 (2017).
49. Hahn, C. & Schwartz, M.A. Mechanotransduction in vascular physiology and atherogenesis. *Nat Rev Mol Cell Biol* **10**, 53-62 (2009).

50. Elton, T.S. & Martin, M.M. Angiotensin II type 1 receptor gene regulation: transcriptional and posttranscriptional mechanisms. *Hypertension* **49**, 953-961 (2007).
51. Galie, P.A., van Oosten, A., Chen, C.S. & Janmey, P.A. Application of multiple levels of fluid shear stress to endothelial cells plated on polyacrylamide gels. *Lab Chip* **15**, 1205-1212 (2015).
52. Kadohama, T., Nishimura, K., Hoshino, Y., Sasajima, T. & Sumpio, B.E. Effects of different types of fluid shear stress on endothelial cell proliferation and survival. *J Cell Physiol* **212**, 244-251 (2007).
53. Iskratsch, T., Wolfenson, H. & Sheetz, M.P. Appreciating force and shape-the rise of mechanotransduction in cell biology. *Nat Rev Mol Cell Biol* **15**, 825-833 (2014).
54. Hughes, J.W., Watkins, L., Blumenthal, J.A., Kuhn, C. & Sherwood, A. Depression and anxiety symptoms are related to increased 24-hour urinary norepinephrine excretion among healthy middle-aged women. *J Psychosom Res* **57**, 353-358 (2004).
55. Li, S.C.*, et al.* Tissue elasticity bridges cancer stem cells to the tumor microenvironment through microRNAs: implications for a "watch-and-wait" approach to cancer. *Curr Stem Cell Res Ther* **12**, 455-470 (2017).
56. Kishi, T., Hirooka, Y. & Sunagawa, K. Sympathoinhibition caused by orally administered telmisartan through inhibition of the AT(1) receptor in the rostral ventrolateral medulla of hypertensive rats. *Hypertens Res* **35**, 940-946 (2012).
57. Huang, N. & Bonn, D. Viscosity of a dense suspension in Couette flow. *J Fluid Mech* **590**, 497-507 (2007).
58. Sugiyama, S.*, et al.* Computational simulation of convection-enhanced drug delivery in the non-human primate brainstem: a simple model predicting the drug distribution. *Neurol Res* **35**, 773-781 (2013).
59. Yao, W., Shen, Z. & Ding, G. Simulation of interstitial fluid flow in ligaments: comparison among Stokes, Brinkman and Darcy models. *Int J Biol Sci* **9**, 1050-1056 (2013).
60. Tarbell, J.M. & Shi, Z.-D. Effect of the glycocalyx layer on transmission of interstitial flow shear stress to embedded cells. *Biomech Model Mechanobiol* **12**, 111-121 (2013).
61. Sakai, K.*, et al.* Overexpression of eNOS in NTS causes hypotension and bradycardia in vivo. *Hypertension* **36**, 1023-1028 (2000).
62. Kishi, T.*, et al.* Overexpression of eNOS in the RVLM causes hypotension and bradycardia via GABA release. *Hypertension* **38**, 896-901 (2001).
63. Paxinos, G. & Watson, C. *The rat brain in stereotaxic coordinates* (Academic Press, 1998).
64. Hirooka, Y., Polson, J.W. & Dampney, R.A. Pressor and sympathoexcitatory effects of nitric oxide in the rostral ventrolateral medulla. *J Hypertens* **14**, 1317-1324 (1996).
65. Shinohara, Y.*, et al.* Effects of neutralizing antibody production on AAV-PHP.B-mediated transduction of the mouse central nervous system. *Mol Neurobiol* **56**, 4203-4214 (2019).

66. Shinohara, Y., Ohtani, T., Konno, A. & Hirai, H. Viral vector-based evaluation of regulatory regions in the neuron-specific enolase (NSE) promoter in mouse cerebellum in vivo. *Cerebellum* **16**, 913-922 (2017).
67. Konno, A.*, et al.* Mutant ataxin-3 with an abnormally expanded polyglutamine chain disrupts dendritic development and metabotropic glutamate receptor signaling in mouse cerebellar Purkinje cells. *Cerebellum* **13**, 29-41 (2014).
68. Matsuzaki, Y.*, et al.* Neurotropic Properties of AAV-PHP.B are shared among diverse inbred strains of mice. *Mol Ther* **27**, 700-704 (2019).
69. Sakitani, N.*, et al.* Application of consistent massage-kike perturbations on mouse calves and monitoring the resulting intramuscular pressure changes. *J Vis Exp* e59475 (2019).
70. Liu, C., De Luca, A., Rosso, A. & Talon, L. Darcy's law for yield stress fluids. *Phys Rev Lett* **122**, 245502 (2019).
71. Schildge, S., Bohrer, C., Beck, K. & Schachtrup, C. Isolation and culture of mouse cortical astrocytes. *J Vis Exp* e50079 (2013).
72. Umemura, S.*, et al.* The Japanese Society of Hypertension guidelines for the management of hypertension (JSH 2019). *Hypertens Res* **42**, 1235-1481 (2019).

Figures and figure legends

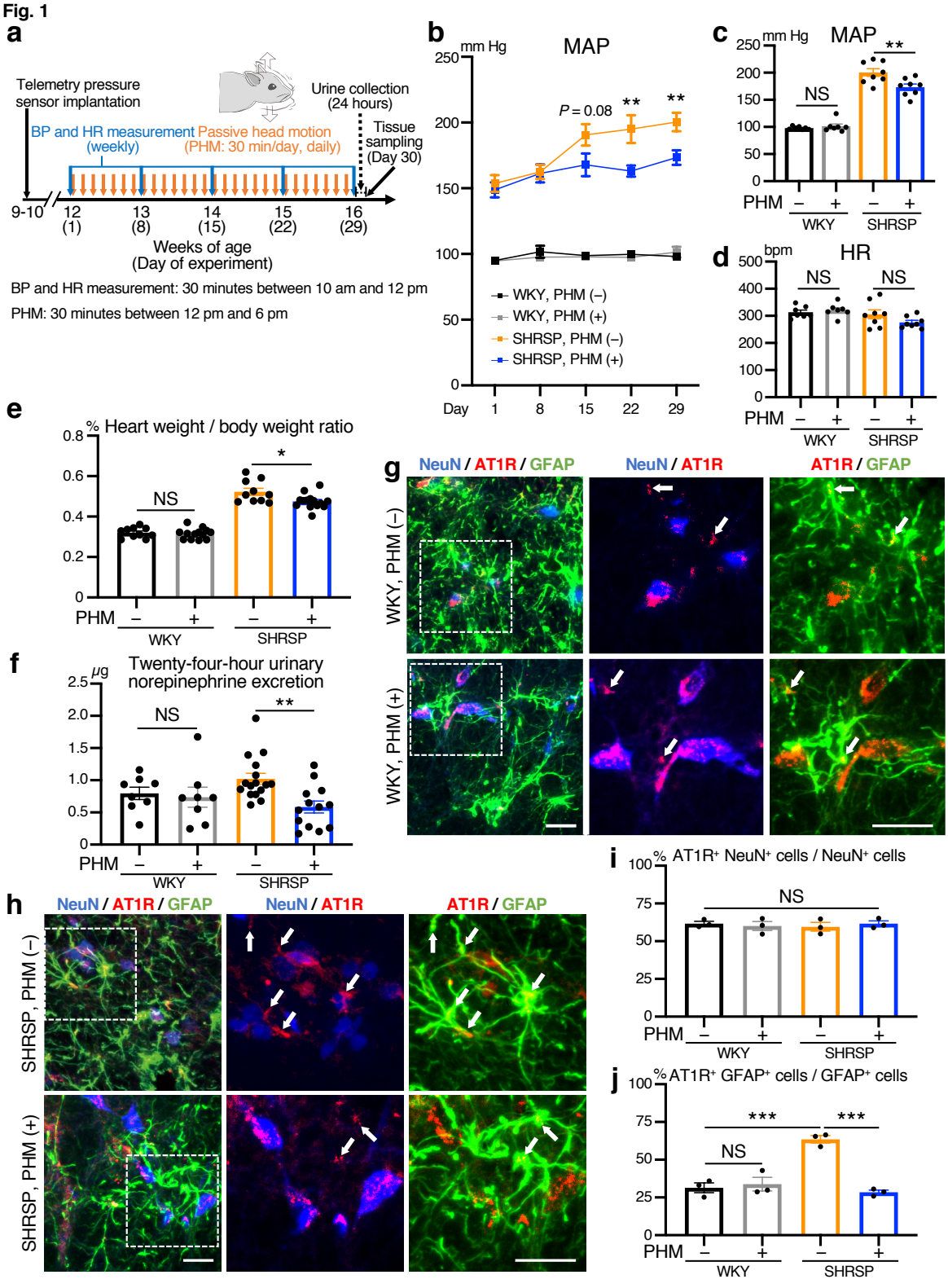

Fig. 1 | Application of cyclical mechanical impact to the head by passive motion lowers the BP

in SHRSPs, and AT1R expression in their RVLM astrocytes. a, Schematic representation of experimental protocol for analysis of the effects of PHM on BP in rats. **b,c,** Time courses **(b)** and values on Day 29 **(c)** of MAP of WKY rats and SHRSPs, subjected to either daily PHM or anesthesia only (**b**: $P = 0.0814$ for Day15, $P = 0.0052$ for Day 22, and $P = 0.0046$ for Day 29. **c**: $P = 0.9739$ for column 1 vs. 2 and $P = 0.0046$ for column 3 vs. 4. $n = 7$ rats for each group of WKY and $n = 8$ rats for each group of SHRSP). **d,** HR values on Day 29 ($P = 0.9650$ for column 1 vs. 2 and $P = 0.2362$ for column 3 vs. 4. $n = 7$ rats for each group of WKY and $n = 8$ rats for each group of SHRSP). **e,** Relative heart weight (heart weight / whole body weight) measured on Day 30 [$P = 0.9866$ for column 1 vs. 2 and $P = 0.0152$ for column 3 vs. 4. $n = 10$ rats for WKY, PHM (−); $n = 13$ rats for WKY, PHM (+); $n = 10$ rats for SHRSP, PHM (−); $n = 14$ rats for SHRSP, PHM (+)]. **f,** Twenty-four-hour (Day 29 to Day 30) urinary norepinephrine excretion [$P = 0.9854$ for column 1 vs. 2 and $P = 0.0085$ for column 3 vs. 4. $n = 8$ rats for each group of WKY; $n = 16$ rats for SHRSP, PHM (−); $n = 13$ rats for SHRSP, PHM (+)]. **g,h,** Micrographic images of anti-NeuN (blue), anti-GFAP (green) and anti-AT1R (red) immunostaining of the RVLM of WKY rats **(g)** and SHRSPs **(h)**, either left sedentary (top) or subjected to PHM (bottom) under anesthesia (30 minutes/day, 28 days). Higher magnification images (center and right) refer to the areas indicated by dotted rectangles in low magnification images (left). Arrows point to anti-AT1R immunosignals that overlap with anti-GFAP, but not anti-NeuN, immunosignals in merged images. Scale bars, 50 μm.

Images are representative of three rats. **i,j,** Quantification of AT1R-positive neurons **(i)** and astrocytes **(j)** in the RVLM of WKY rats and SHRSPs, either left sedentary or subjected to PHM. Fifty NeuN-positive ($NeuN^+$) cells and one hundred GFAP-positive ($GFAP^+$) cells were analyzed for each rat (**i**: $P = 0.7803$. **j**: $P = 0.9455$ for column 1 vs. 2, $P = 0.0004$ for column 1 vs. 3, and $P = 0.0002$ for column 3 vs. 4. $n = 3$ rats for each group). Data are presented as mean ± s.e.m. $^{*}P < 0.05$; $^{**}P < 0.01$; $^{***}P < 0.001$; NS, not significant; one-way ANOVA with Tukey's post hoc multiple comparisons test.

Extended Data Fig. 1

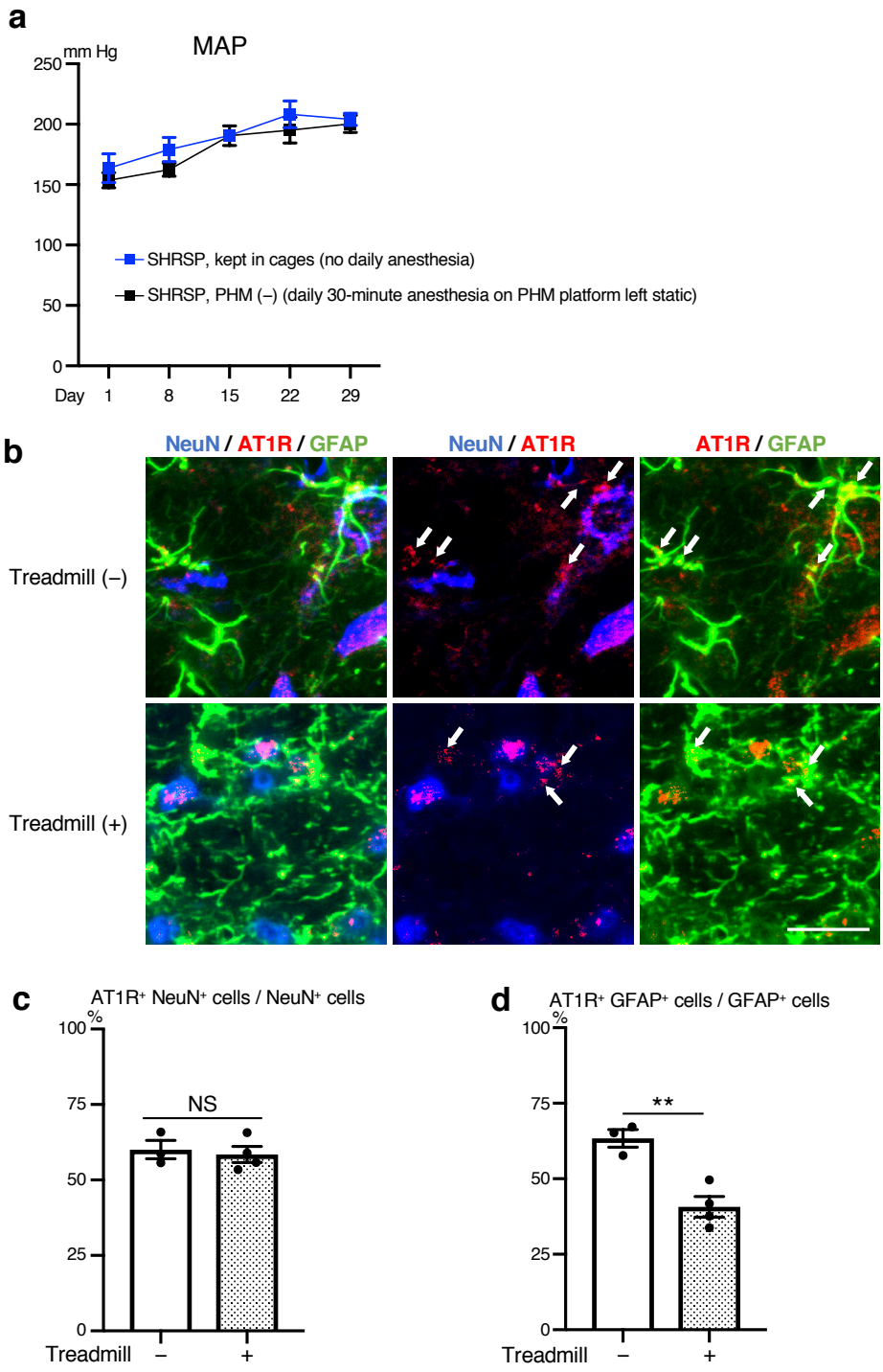

Extended Data Fig. 1 | Daily anesthesia alone does not affect BP, and treadmill running decreases AT1R expression in the RVLM astrocytes in SHRSPs. a, Time courses of MAP of

SHRSPs either routinely kept in cages (no anesthesia) or subjected to daily anesthesia on the platform of PHM machine without turning on its switch [PHM (−)] [n = 6 rats for no daily anesthesia and n = 8 rats for PHM (−)]. **b,** Micrographic images anti-NeuN (blue), anti-GFAP (green) and anti-AT1R (red) immunostaining of the RVLM of SHRSPs, either placed in the static treadmill machine or subjected to treadmill running at the velocity of 20 m/minute (30 minutes/day, 28 days). Arrows point to anti-AT1R immunosignals that overlap with anti-GFAP, but not anti-NeuN, immunosignals in merged images. Scale bar, 50 μm. Images are representative of three or four rats. **c,d,** Quantification of AT1R-positive neurons **(c)** and astrocytes **(d)** in the RVLM of SHRSPs with or without 4-week treadmill running. Fifty $NeuN^+$ cells and one hundred $GFAP^+$ cells were analyzed for each rat [**c**: $P = 0.7056$. **d**: $P = 0.0048$. n = 3 rats for treadmill (−) and n = 4 rats for treadmill (+)]. Data are presented as mean ± s.e.m. $^{**}P < 0.01$; NS, not significant, unpaired two-tailed Student's t-test.

Fig. 2

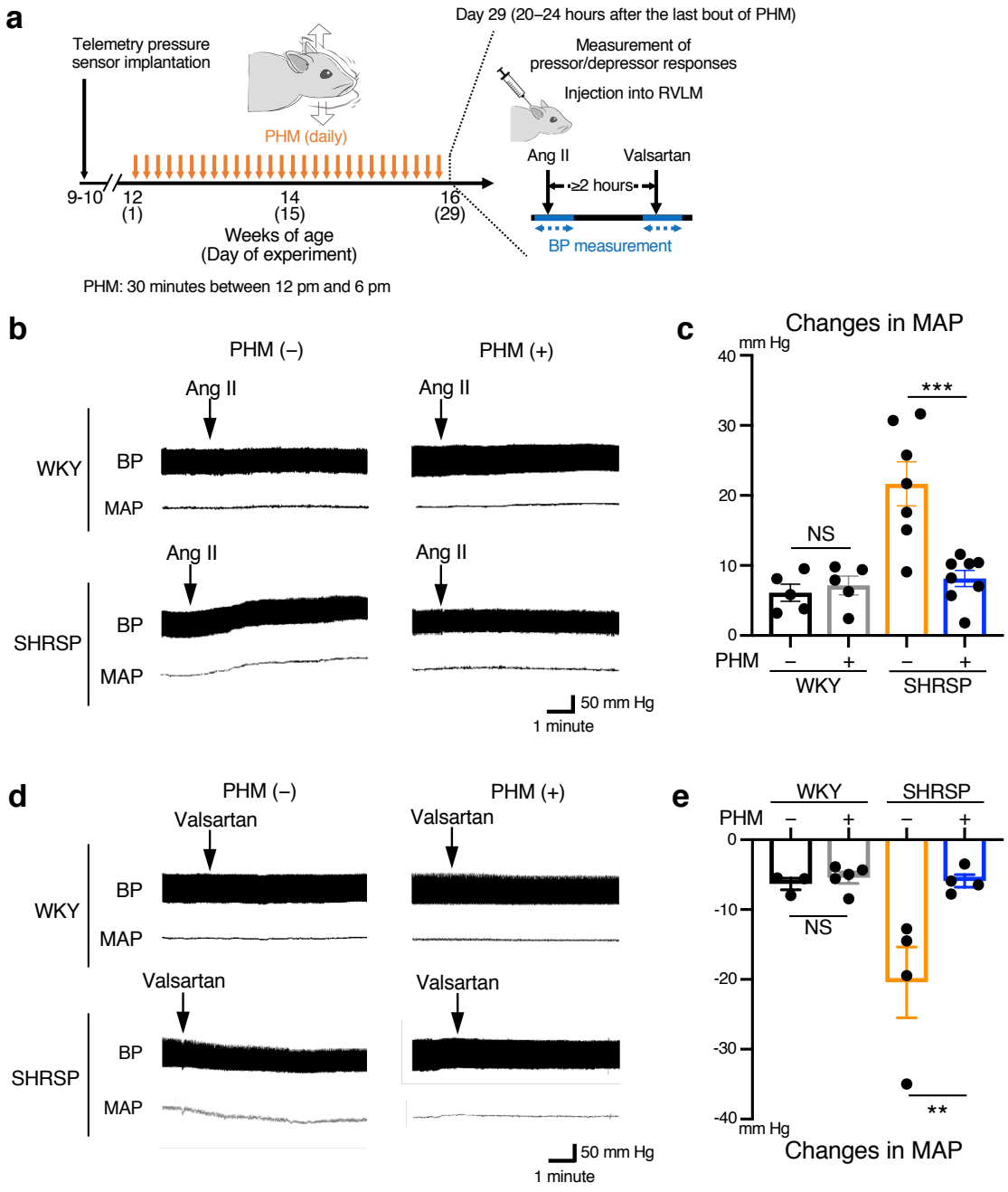

639

640 **Fig. 2 | PHM alleviates the sensitivity of RVLM in SHRSPs to Ang II or valsartan. a,**

641 Schematic representation of experimental protocol for analysis of the effects of PHM on the

642 sensitivity to Ang II or valsartan injected into unilateral RVLM. Ang II (100 pmol) was injected into

643 the unilateral RVLM of WKY rats and SHRSPs, either left sedentary (daily anesthesia) or subjected
644 to PHM (30 minutes/day, 28 days), with their BP monitored under urethane anesthesia. Injection of
645 valsartan (100 pmol) into the RVLM was conducted at least 2 hours after the injection of Ang II. **b,**
646 Representative trajectories of BP (top in each panel) and MAP (bottom in each panel). Arrows point
647 to the time of the initiation of RVLM injection of Ang II. **c,** Quantification of MAP change caused
648 by Ang II injection [$P = 0.9876$ for column 1 vs. 2 and $P = 0.0003$ for column 3 vs. 4. $n = 5$ rats for
649 each group of WKY; $n = 7$ rats for SHRSP, PHM (−); $n = 8$ rats for SHRSP, PHM (+)]. **d,e,** Effects
650 of RVLM injection of valsartan (100 pmol) examined as in **(b,c)** [**e**: $P = 0.9953$ for column 1 vs. 2
651 and $P = 0.0099$ for column 3 vs. 4. $n = 3$ rats for WKY, PHM (−); $n = 5$ rats for WKY, PHM (+); n
652 = 4 rats for each group of SHRSP]. Data are presented as mean ± s.e.m. $^{**}P < 0.01$; $^{***}P < 0.001$;
653 NS, not significant; one-way ANOVA with Tukey's post hoc multiple comparisons test.

Fig. 3

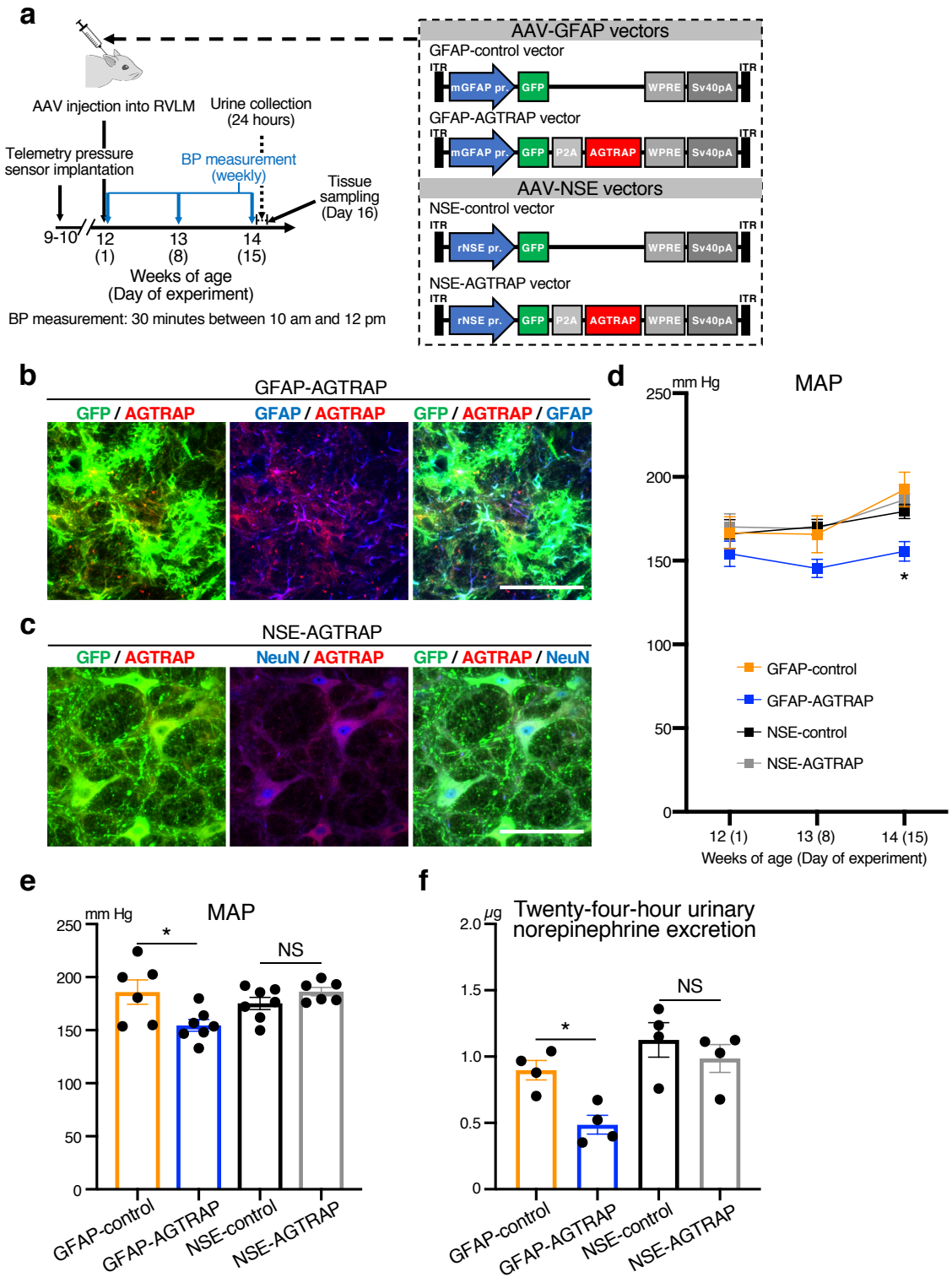

Fig. 3 | AAV-mediated expression of AGTRAP in RVLM astrocytes, but not neurons, lowers

656 **the BP in SHRSPs. a,** Schematic representation of experimental protocol for analysis of the effects
657 of AAV-mediated transduction of RVLM astrocytes or neurons with AGTRAP gene. ITR; inverted
658 terminal repeat. **b,c,** Astrocyte- **(b)** and neuron- **(c)** specific transgene expression by RVLM
659 injection of AAV9 vectors. Micrographic images of GFP (green) and anti-GFAP **(b)** or anti-NeuN
660 **(c)** immunostaining (blue) of RVLM of SHRSPs 15 days after the injection of AAV9 vectors
661 indicated at the top of each panel. Scale bars, 50 μm. Images are representative of three rats. **d−f,**
662 Time courses **(d)** and values on Day 15 **(e)** of MAP (**d**: $P = 0.0229$ for Day 14. **e**: $P = 0.0229$ for
663 column 1 vs. 2 and $P = 0.6864$ for column 3 vs. 4. $n = 6$ rats for GFAP-control; $n = 7$ rats for
664 GFAP-AGTRAP; $n = 7$ rats for NSE-control; $n = 6$ rats for NSE-AGTRAP), and 24-hour urinary
665 norepinephrine excretion **(f)** ($P = 0.0497$ for column 1 vs. 2 and $P = 0.7455$ for column 3 vs. 4. $n =$
666 4 rats for each group) of SHRSPs subjected to RVLM injection of AAV9 vectors. Data are
667 presented as mean ± s.e.m. *$P < 0.05$; NS, not significant, one-way ANOVA with Tukey's post hoc
668 multiple comparisons test.

Extended Data Fig. 2

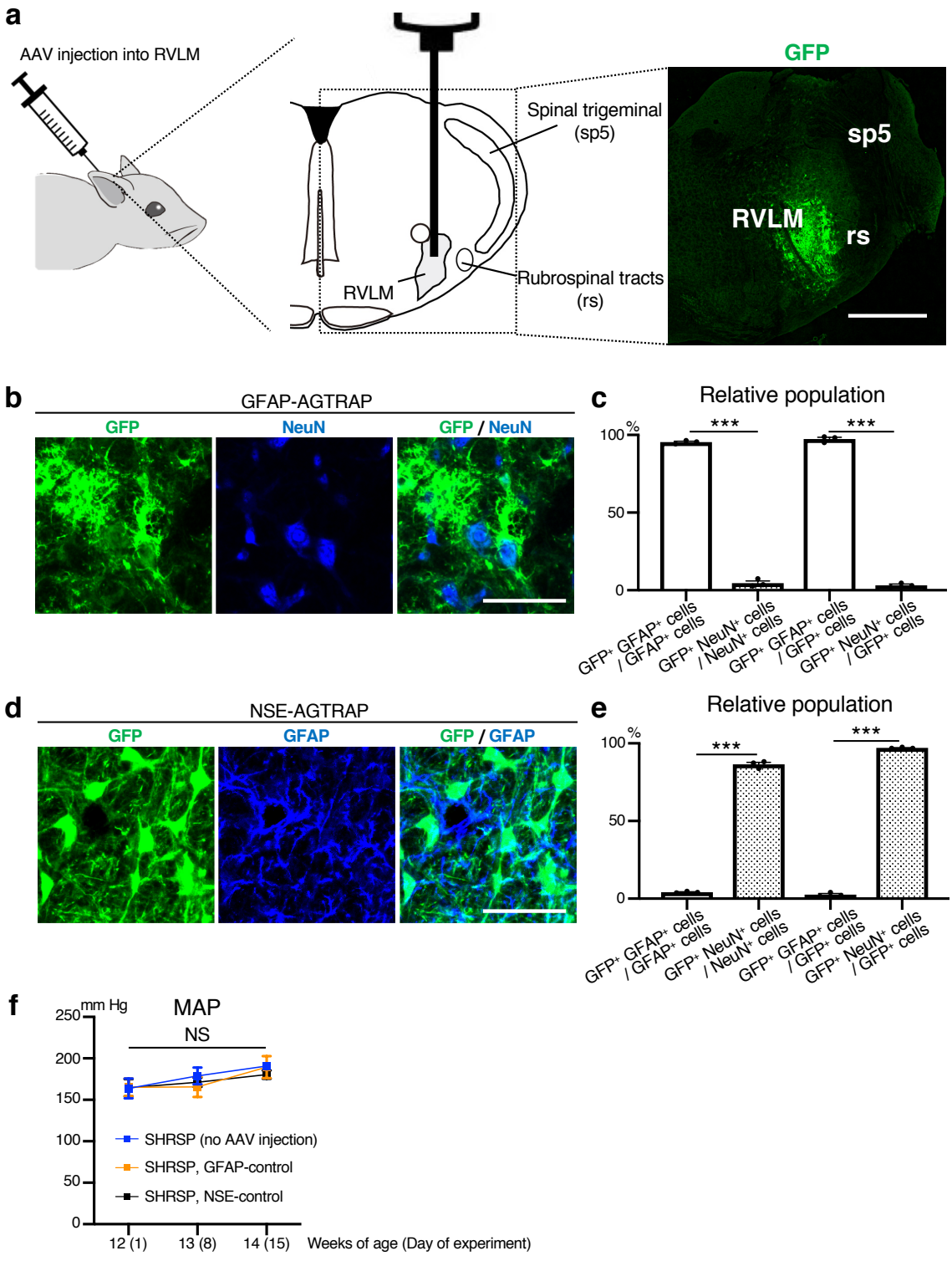

Extended Data Fig. 2 | AAV-mediated transduction of RVLM astrocytes or neurons in

SHRSPs. a, Schematic representation of injection of AAV9 vectors to RVLM. Micrographic image is representative of three rats analyzed in Fig. 3b (15 days after the RVLM injection of GFAP-AGTRAP vector). GFP-derived fluorescence indicates cells expressing the transgene. Scale bar, 1 mm. **b,c,** Efficiency and specificity of astrocyte-specific expression of the transgene. **(b)** Micrographic images of GFP (green) and anti-NeuN immunostaining (blue) of RVLM of SHRSPs analyzed in Fig. 3b. Scale bar, 50 μm. Images are representative of three rats. **(c)** Quantification of the efficiency and specificity of transgene expression. The relative populations (%) of GFP- GFAP-double positive (GFP^+ $GFAP^+$) or GFP- NeuN-double positive (GFP^+ $NeuN^+$) cells were calculated by referring their numbers to those of GFP^+, $GFAP^+$ or $NeuN^+$ cells ($P < 0.0001$ for column 1 vs. 2 and $P < 0.0001$ for column 3 vs. 4. $n = 3$ rats for each group). **d,e,** Efficiency and specificity of neuron-specific expression of the transgene. **(d)** Micrographic images of GFP (green) and anti-GFAP immunostaining (blue) of RVLM of SHRSPs analyzed in Fig. 3c. Scale bar, 50 μm. Images are representative of three rats. **(e)** The efficiency and specificity quantified as in **(c)** ($P < 0.0001$for column 1 vs. 2 and $P < 0.0001$ for column 3 vs. 4.). **f,** BP in SHRSPs injected with control vectors. BP was measured and MAP was quantified as in Fig. 1b ($P = 0.9803$ for Week 12, $P = 0.5914$ for Week 13, and $P = 0.4693$ for Week 14. $n = 6$ rats for no AAV injection; $n = 6$ rats for GFAP-control; $n = 7$ rats for NSE-control). The data for blue line are identical with those demonstrated with blue line in Extended Data Fig. 1a. Data are presented as mean ± s.e.m. ***$P < 0.001$; NS, not

689 significant; unpaired two-tailed Student's *t*-test **(c,e)** or one-way ANOVA with Tukey's post hoc

690 multiple comparisons test **(f)**.

Fig. 4

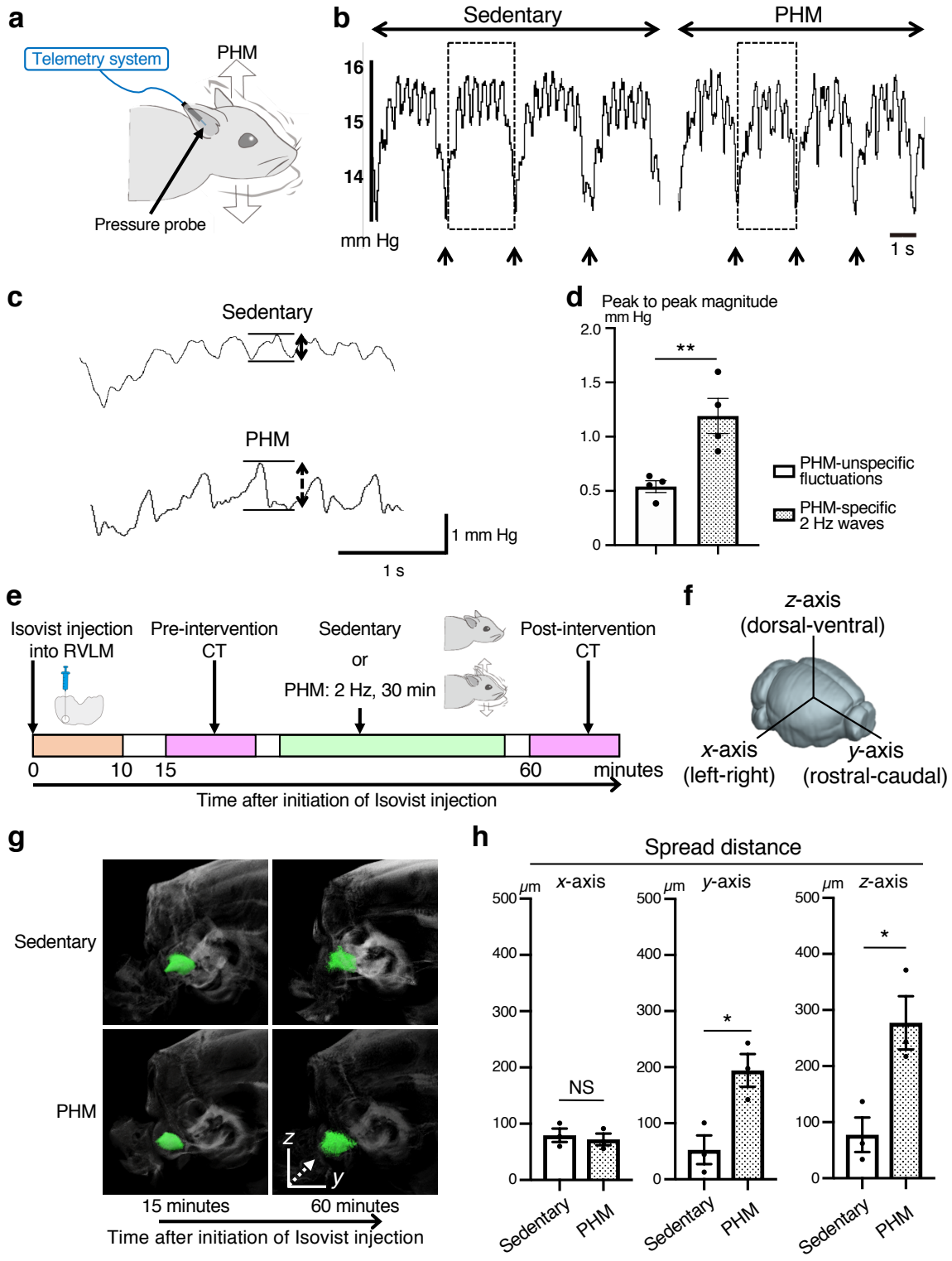

691

692 **Fig. 4 | PHM generates pressure waves of low amplitude, but facilitates interstitial fluid**

693 **movement (flow) in rat RVLM. a,** Schematic representation of pressure measurement in rat
694 RVLM. **b,** Representative pressure waves recorded in rat RVLM during sedentary condition and
695 PHM. Arrows point to the time of transition from inhalation to exhalation detected by simultaneous
696 respiration monitoring. Scale bar, 1 s. Images are representative of three independent experiments
697 with similar results. **c,** Respiration-unsynchronized pressure changes. Respiration-synchronized
698 pressure waves indicated by dotted rectangles in **(b)** are presented with high magnification. Right-
699 angled scale bar, 1 s / 1 mm Hg. Note that 2-Hz pressure waves indicated by a two-headed dotted
700 line arrow were specifically generated during PHM. **d,** Magnitude of PHM-specific and -unspecific
701 pressure changes unsynchronized with respiration. Peak to peak magnitudes indicated by two-
702 headed arrows in **(c)** were quantified ($P = 0.0089$. $n = 4$ rats for each group, 10 segments analyzed
703 for each rat). **e,** Schematic representation of experimental protocol for μCT analysis of Isovist
704 injected in rat RVLM. **f,** Definition of *x*-(left-right), *y*-(rostral-caudal), and *z*-(dorsal-ventral) axes
705 used in this study. **g,** Representative Isovist spreading presented on X-ray images. Isovist clusters
706 are indicated by green. Images are representative of three rats. A dotted line arrow indicates the
707 main direction of spreading in this sample. **h,** Quantification of Isovist spreading along each axis
708 (left chart: $P = 0.6666$. middle chart: $P = 0.0218$. right chart: $P = 0.0244$. $n = 3$ rats for each group).
709 Data are presented as mean ± s.e.m. $^{*}P < 0.05$; $^{**}P < 0.01$; NS, not significant, unpaired two-tailed
710 Student's *t*-test.

Supplementary Table 1

a

Property	Value
Pressure changes (ΔP; mmHg)	1.19
Viscosity (μ; mPa•s)	1–20 ♯
Spread distance along *x*-axis per each PHM cycle (Δx; μm)	–0.002
Spread distance along *y*-axis per each PHM cycle (Δy; μm)	0.039
Spread distance along *z*-axis per each PHM cycle (Δz; μm)	0.055
Velocity of interstitial fluid flow along *x*-axis ($u_{\infty,x}$; μm/s)	–0.004
Velocity of interstitial fluid flow along *y*-axis ($u_{\infty,y}$; μm/s)	0.079
Velocity of interstitial fluid flow along z-axis ($u_{\infty,z}$; μm/s)	0.111

b

FSS (τ_x) along *x*-axis at the cell surface:

$$\tau_x = \frac{\mu u_{\infty,x}}{\sqrt{K_{p,x}}}$$

$$K_{p,x} = \frac{\mu u_{\infty,x} \Delta x}{\Delta P}$$

, where $K_{p,x}$ is the Darcy permeability of brain tissue along *x*-axis.

The shear stresses along *y*- and *z*-axes can be calculated in a similar manner.

When the values listed in **a** are introduced in these equations, the magnitude of FSS is estimated as 0.59–2.64 Pa.

Supplementary Table 1 | Simulative calculation of the magnitude of PHM-generated FSS on rat RVLM cells. a, Values referenced for simulative calculation of the magnitude of FSS that PHM generated in rat RVLM. All referenced values except viscosity (marked with ♯) were drawn from

analyses with IBP measurement and Isovist-enhanced μCT scanning (Fig. 4d,h). The property of interstitial fluid viscosity was referenced from previous studies[57-59]. **b,** Calculation of the magnitude of FSS generated by PHM. FSS (τ) at the cell surface can be calculated as reported previously[60].

Fig. 5

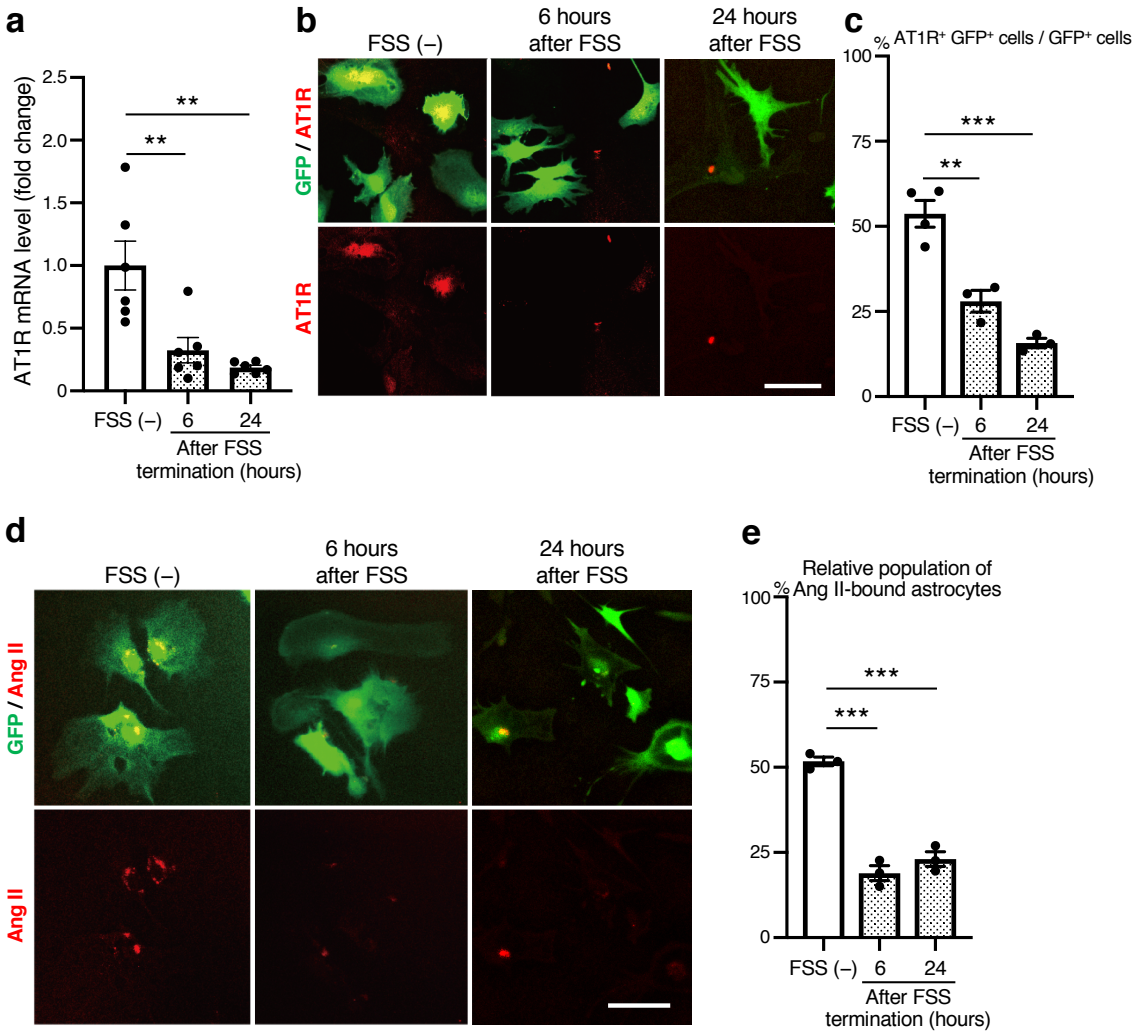

Fig. 5 | FSS on cultured astrocytes decreases their AT1R expression and Ang II-binding potential in vitro. a–c, AT1R expression in cultured astrocytes with or without exposure to FSS. Astrocytes prepared from astrocyte-GFP mice, either left unexposed or exposed to pulsatile FSS (average 0.7 Pa, 0.5 Hz, 30 minutes) were analyzed 6 and 24 hours after the cessation of 30-minute FSS application. **(a)** AT1R mRNA expression levels normalized against GAPDH expression and scaled as the mean value from control samples (cells left unexposed to FSS) set as 1 ($P = 0.0050$ for

column 1 vs. 2 and $P = 0.0011$ for column 1 vs. 3. $n = 6$). **(b)** Microscopic images of anti-AT1R (red) and anti-GFP (green) immunostaining. Images are representative of three or four independent experiments with similar results. Scale bar, 50 μm. **(c)** Relative population of AT1R- GFP-double positive ($AT1R^+$ GFP^+) cells were quantified as a ratio to total GFP-positive (GFP^+) cells in each sample [$P = 0.0021$ for column 1 vs. 2 and $P = 0.0002$ for column 1 vs. 3. >100 GFP-positive cells were analyzed in each sample; $n = 4$ for FSS (−), $n = 3$ for 6 and 24 hours after FSS]. **d,e,** Effect of FSS on astrocytes' Ang II-binding potential. Cultured astrocytes were either left unexposed or exposed to FSS as in **(a−c)**. Six and twenty-four hours after the cessation of 30-minute FSS application, cells were subjected to fluorescent Ang II binding assay. **(d)** Microscopic images representative of three independent experiments with similar results. Scale bar, 50 μm. **(e)** GFP-positive cells with punctate red fluorescence (TAMRA-Ang II-bound astrocytes) were quantified as a ratio (%) to total GFP-positive cells in each sample ($P < 0.0001$ for column 1 vs. 2 and $P = 0.0001$ for column 1 vs. 3. 100 GFP-positive cells were analyzed in each sample; $n = 3$ for each group). Data are presented as mean ± s.e.m. $^{**}P < 0.01$, $^{***}P < 0.001$, one-way ANOVA with Tukey's post hoc multiple comparisons test.

Extended Data Fig. 3

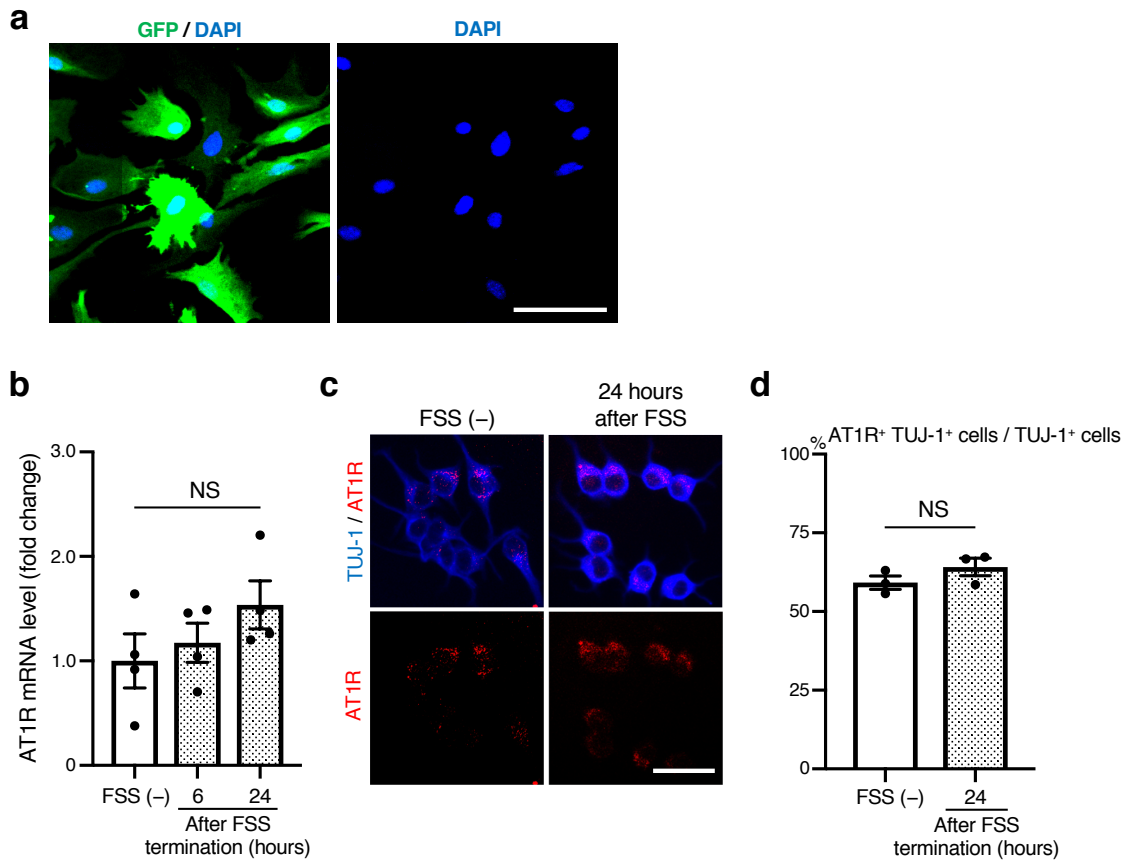

Extended Data Fig. 3 | Preparation of astrocyte-enriched primary culture, and lack of decreasing effect of FSS on AT1R expression in cultured neuronal cells. a, Representative micrographic image of anti-GFP immunostaining (green) and DAPI staining (blue) of astrocyte-enriched culture prepared from astrocyte-GFP mice. Scale bar, 50 μm. Note that most of the cells are GFP-positive. **b–d,** Effects of FSS on AT1R expression in Neuro2A cells analyzed as in Fig. 5a–c. **(b)** AT1R mRNA expression levels ($P = 0.2834$. $n = 4$). **(c)** Micrographic images representative of three independent experiments with similar results. Scale bar, 50 μm. **(d)** Relative population of AT1R- TUJ-1-double positive ($AT1R^+$ $TUJ\text{-}1^+$) cells quantified as a ratio to total TUJ-

749 1-positive (TUJ-1^{+}) cells in each sample (P = 0.2308. >100 TUJ-1-positive cells were analyzed in

750 each sample; n = 3). Data are presented as mean ± s.e.m. NS, not significant, one-way ANOVA with

751 Tukey's post hoc multiple comparisons test **(b)** or unpaired two-tailed Student's *t*-test **(d)**.

Fig. 6

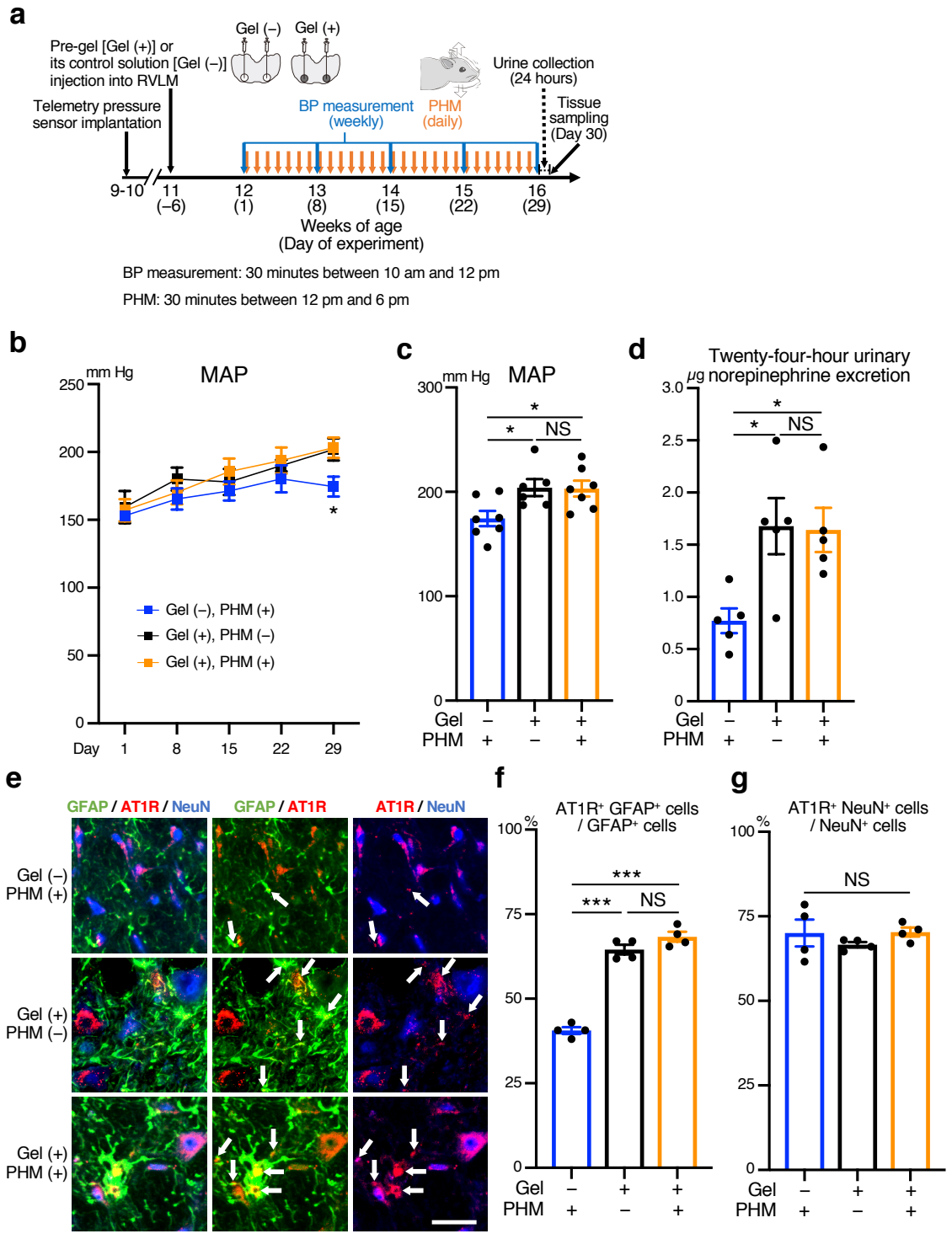

Fig. 6 | Hydrogel introduction eliminates decreasing effects of PHM on BP and AT1R expression in the RVLM astrocytes in SHRSPs. a, Schematic representation of experimental

protocol for analysis of the effects of PHM with and without PEG hydrogel introduction in bilateral RVLMs of SHRSPs. PHM was applied daily for consecutive 28 days. **b−d,** Time courses **(b)** and values on Day 29 **(c)** of MAP, and 24-hour urinary norepinephrine excretion **(d)** of SHRSPs, subjected to various combinations of daily PHM application and hydrogel introduction in bilateral RVLMs. Note the absence of significant difference in BP **(b,c)** and urinary norepinephrine excretion **(d)** of SHRSPs with hydrogel introduced RVLMs [Gel (+)] between with and without PHM [**b**: P = 0.0372 for Day 29. **c**: P = 0.0387 for column 1 vs. 2, P = 0.0372 for column 1 vs. 3, and P = 0.9959 for column 2 vs. 3. n = 7 rats for Gel (−), PHM (+) and for Gel (+), PHM (+); n = 6 rats for Gel (+), PHM (−); **d**: P = 0.0247 for column 1 vs. 2, P = 0.0307 for column 1 vs. 3, and P = 0.9920 for column 2 vs. 3. n = 5 rats for each group]. **e**, Micrographic images of anti-GFAP (green), anti-AT1R (red), and anti-NeuN (blue) immunostaining of the RVLM in SHRSPs subjected to various combinations of hydrogel introduction in bilateral RVLMs and 4-week PHM application. Arrows point to anti-AT1R immunosignals that overlap with anti-GFAP, but not anti-NeuN, immunosignals in merged images. Scale bar, 50 μm. Images are representative of four rats. **f,g,** Quantification of AT1R-positive astrocytes **(f)** and neurons **(g)** in the RVLM. Note the absence of significant difference in the ratio of AT1R-positive astrocytes of SHRSPs with hydrogel introduced RVLMs [Gel (+)] between with and without PHM (**f**, columns 2 and 3). Fifty $NeuN^+$ cells and one hundred $GFAP^+$ cells were analyzed for each rat (**f**: $P < 0.0001$ for column 1 vs. 2, $P < 0.0001$ for column 1

773 vs. 3, and $P = 0.1597$ for column 2 vs. 3. **g**: $P = 0.5182$. $n = 4$ rats for each group). Data are

774 presented as mean ± s.e.m. *$P < 0.05$; ***$P < 0.001$; NS, not significant, one-way ANOVA with

775 Tukey's post hoc multiple comparisons test.

Extended Data Fig. 4

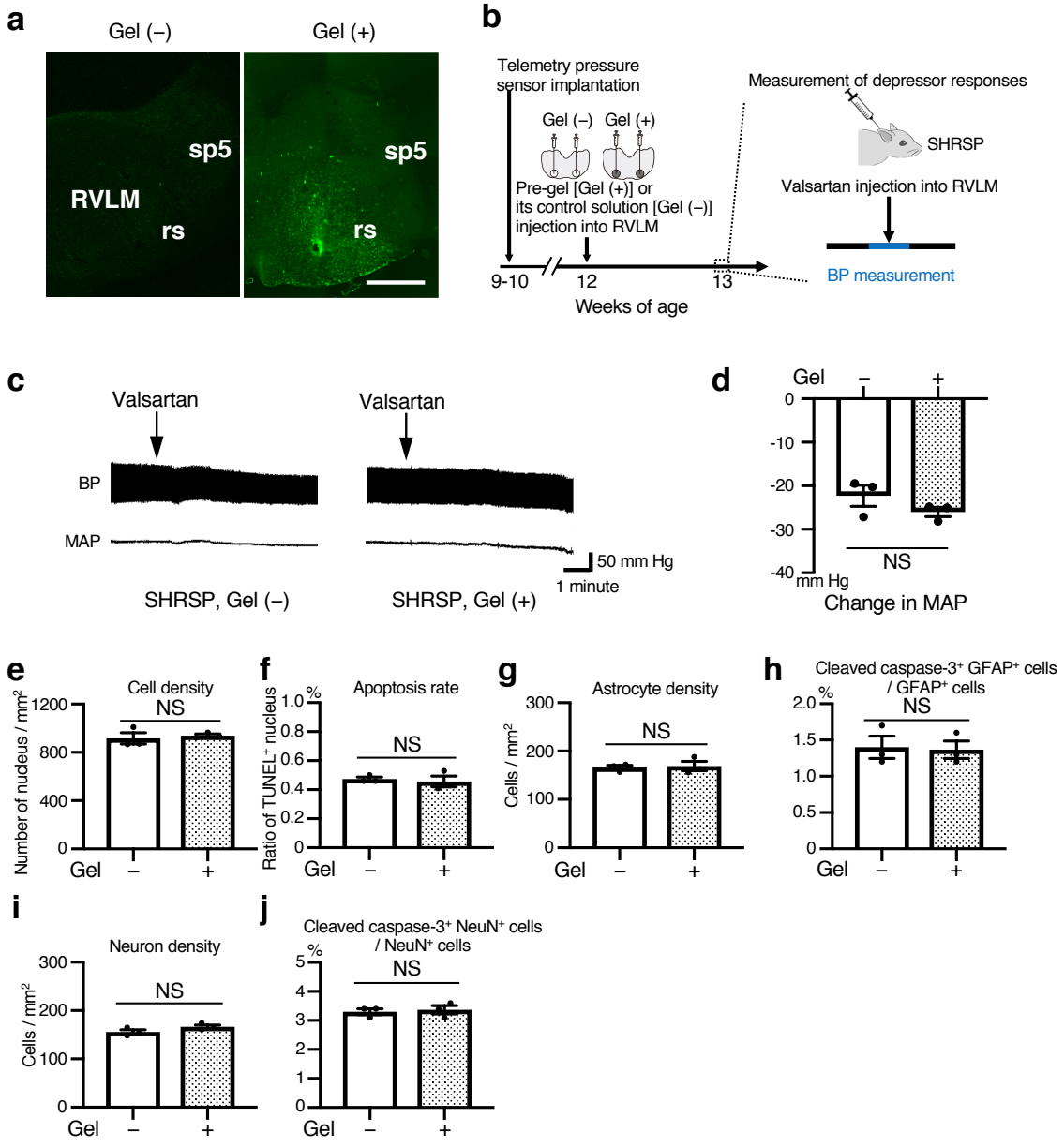

Extended Data Fig. 4 | Hydrogel introduction in the RVLM does not affect the depressor response to valsartan or survival/apoptosis of RVLM astrocytes and neurons in SHRSPs. a, Introduction of PEG hydrogel in rat RVLM. Twenty-four hours after the injection of control ungelatable fluorescent PEG solution (left) or 1 week after the injection of pre-gel fluorescent PEG

781 solution (right), brainstem samples were prepared. Coronal-section images representative of three
782 rats with similar results are shown. Scale bar, 1 mm. **b,** Schematic representation of experimental
783 protocol. One week after the injection of pre-gel PEG solution or its ungelatable control, depressor
784 response was analyzed as in Fig. 2. **c,d,** Representative trajectories **(c)** and quantification **(d)** of BP
785 descent upon valsartan injection to the RVLM of SHRSPs with or without hydrogel introduction (**d**:
786 $P = 0.2342$. $n = 3$ rats for each group). **e–j,** Effects of hydrogel introduction on survival/apoptosis
787 of RVLM cells in SHRSPs. Rat RVLM sections prepared in the experiments for Fig. 6e–g [PHM
788 (+), Gel (−) and PHM (+), Gel (−)] were subjected to TUNEL assay **(e,f)**, or combinations of anti-
789 GFAP, anti-NeuN and anti-cleaved caspase-3 immunostaining **(g–j)**. DAPI-positive nuclei **(e)**,
790 GFAP- **(g)** or NeuN- **(i)** positive cells were counted, and the relative populations of cells doubly
791 positive for indicated combinations of TUNEL **(f)** and cleaved caspase-3 **(h,j)** were quantified. Each
792 value represents an average from five images of 1 x 1-mm area analyzed for each rat (**e**: $P = 0.6518$.
793 **f**: $P = 0.6943$. **g**: $P = 0.7938$. **h**: $P = 0.8722$. **i**: $P = 0.1679$. **j**: $P = 0.7247$. $n = 3$ rats for each group).
794 Data are presented as mean ± s.e.m. NS, not significant; unpaired two-tailed Student's *t*-test.

Fig. 7

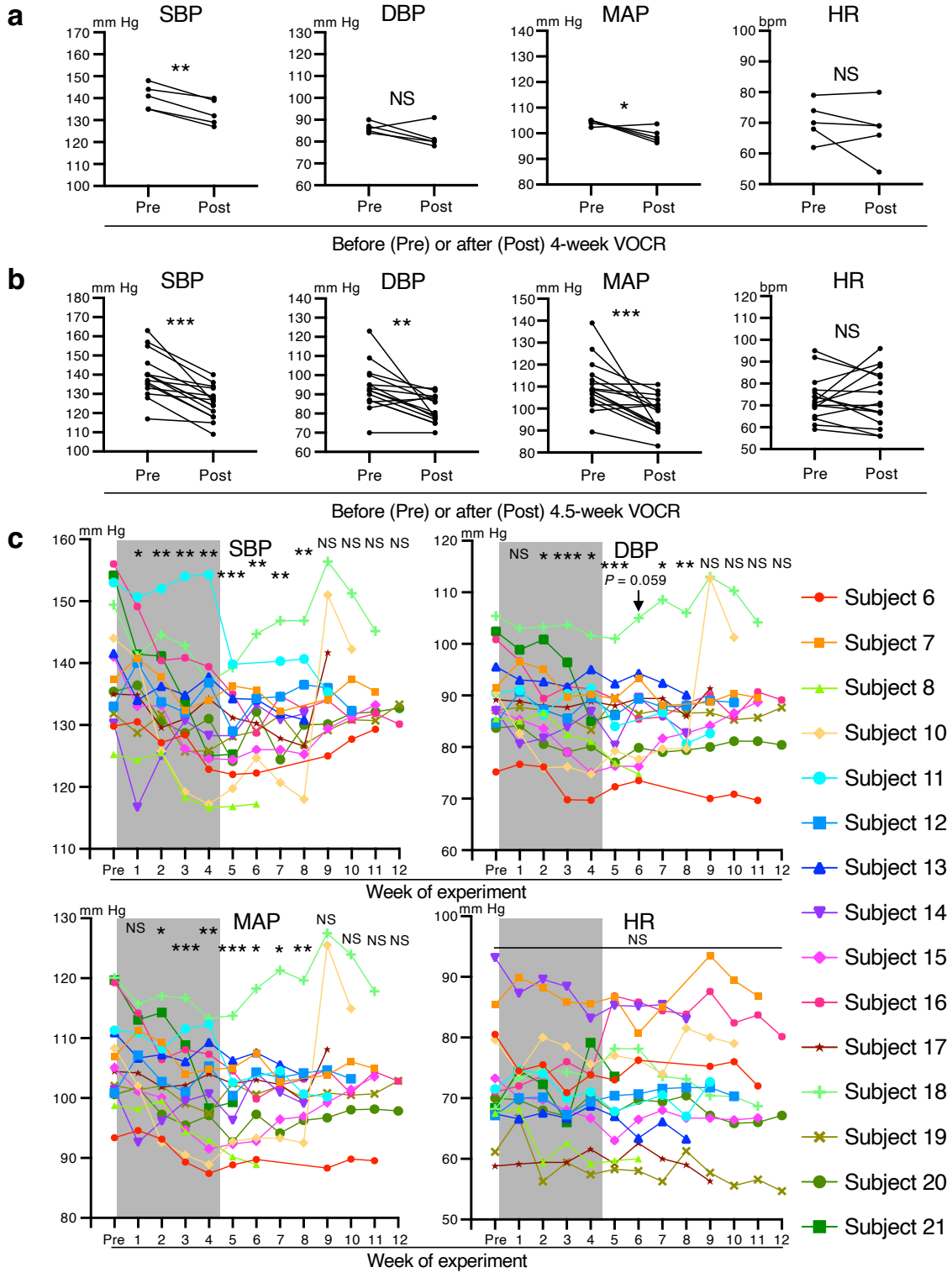

795

796 **Fig. 7 | VOCR has an antihypertensive effect on hypertensive adult humans. a,** BP and HR

797 “value of the day”s immediately before and after 4-week VOCR in the study of protocol 1 (SBP: *P*
798 = 0.0018. DBP: *P* = 0.1509. MAP: *P* = 0.0459. HR: *P* = 0.3900. *n* = 5). **b,** BP and HR “value of the
799 week”s immediately before and after 4.5-week VOCR in the study of protocol 2 (SBP: *P* < 0.0001.
800 DBP: *P* = 0.0031. MAP: *P* = 0.0009. HR: *P* = 0.9817. *n* = 15). **c,** Subject number-corresponding
801 trajectories and statistical analysis of BP and HR in the study of protocol 2. Gray-shaded rectangles
802 indicate the VOCR intervention periods (4.5 weeks). The colors and symbols of individual lines
803 correspond to those of individual subject numbers listed on the right, excluding subject 9 (see
804 Supplementary Table 2). Each “value of the week” was statistically compared with that of the week
805 immediately before the initiation of VOCR intervention (SBP: *P* = 0.0293 for Pre vs. Week 1, *P* =
806 0.00228 for Pre vs. Week 2, *P* = 0.0013 for Pre vs. Week 3, *P* = 0.0035 for Pre vs. Week 4, *P* =
807 0.0002 for Pre vs. Week 5, *P* = 0.0078 for Pre vs. Week 6, *P* = 0.0035 for Pre vs. Week 7, *P* =
808 0.0075 for Pre vs. Week 8, *P* = 0.2132 for Pre vs. Week 9, *P* = 0.1314 for Pre vs. Week 10, *P* =
809 0.0973 for Pre vs. Week 11, and *P* = 0.3993 for Pre vs. Week 12. DBP: *P* = 0.3022 for Pre vs. Week
810 1, *P* = 0.0436 for Pre vs. Week 2, *P* = 0.0010 for Pre vs. Week 3, *P* = 0.0100 for Pre vs. Week 4, *P* =
811 0.0006 for Pre vs. Week 5, *P* = 0.0599 for Pre vs. Week 6, *P* = 0.0488 for Pre vs. Week 7, *P* =
812 0.0096 for Pre vs. Week 8, *P* = 0.9346 for Pre vs. Week 9, *P* = 0.7850 for Pre vs. Week 10, *P* =
813 0.0769 for Pre vs. Week 11, and *P* = 0.3137 for Pre vs. Week 12. MAP: *P* = 0.1075 for Pre vs. Week
814 1, *P* = 0.0132 for Pre vs. Week 2, *P* = 0.0008 for Pre vs. Week 3, *P* = 0.0063 for Pre vs. Week 4, *P* =

0.0003 for Pre vs. Week 5, $P = 0.0251$ for Pre vs. Week 6, $P = 0.0136$ for Pre vs. Week 7, $P = 0.0071$ for Pre vs. Week 8, $P = 0.6795$ for Pre vs. Week 9, $P = 0.4295$ for Pre vs. Week 10, $P = 0.0704$ for Pre vs. Week 11, and $P = 0.3662$ for Pre vs. Week 12. HR: $P = 0.6287$ for Pre vs. Week 1, $P = 0.7840$ for Pre vs. Week 2, $P = 0.1573$ for Pre vs. Week 3, $P = 0.5380$ for Pre vs. Week 4, $P = 0.7331$ for Pre vs. Week 5, $P = 0.6995$ for Pre vs. Week 6, $P = 0.9110$ for Pre vs. Week 7, $P = 0.9875$ for Pre vs. Week 8, $P = 0.5866$ for Pre vs. Week 9, $P = 0.9566$ for Pre vs. Week 10, $P = 0.6487$ for Pre vs. Week 11, and $P = 0.9905$ for Pre vs. Week 12. $n = 15$ for Pre and Weeks 1 to 5, $n = 13$ for Week 6, $n = 12$ for Week 7, $n = 11$ for Weeks 8 and 9, $n = 9$ for Week 10, $n = 7$ for Week 11, $n = 3$ for Week 12). $^{*}P < 0.05$; $^{**}P < 0.01$; $^{***}P < 0.001$; NS, not significant, paired two-tailed Student's *t*-test.

Extended Data Fig. 5

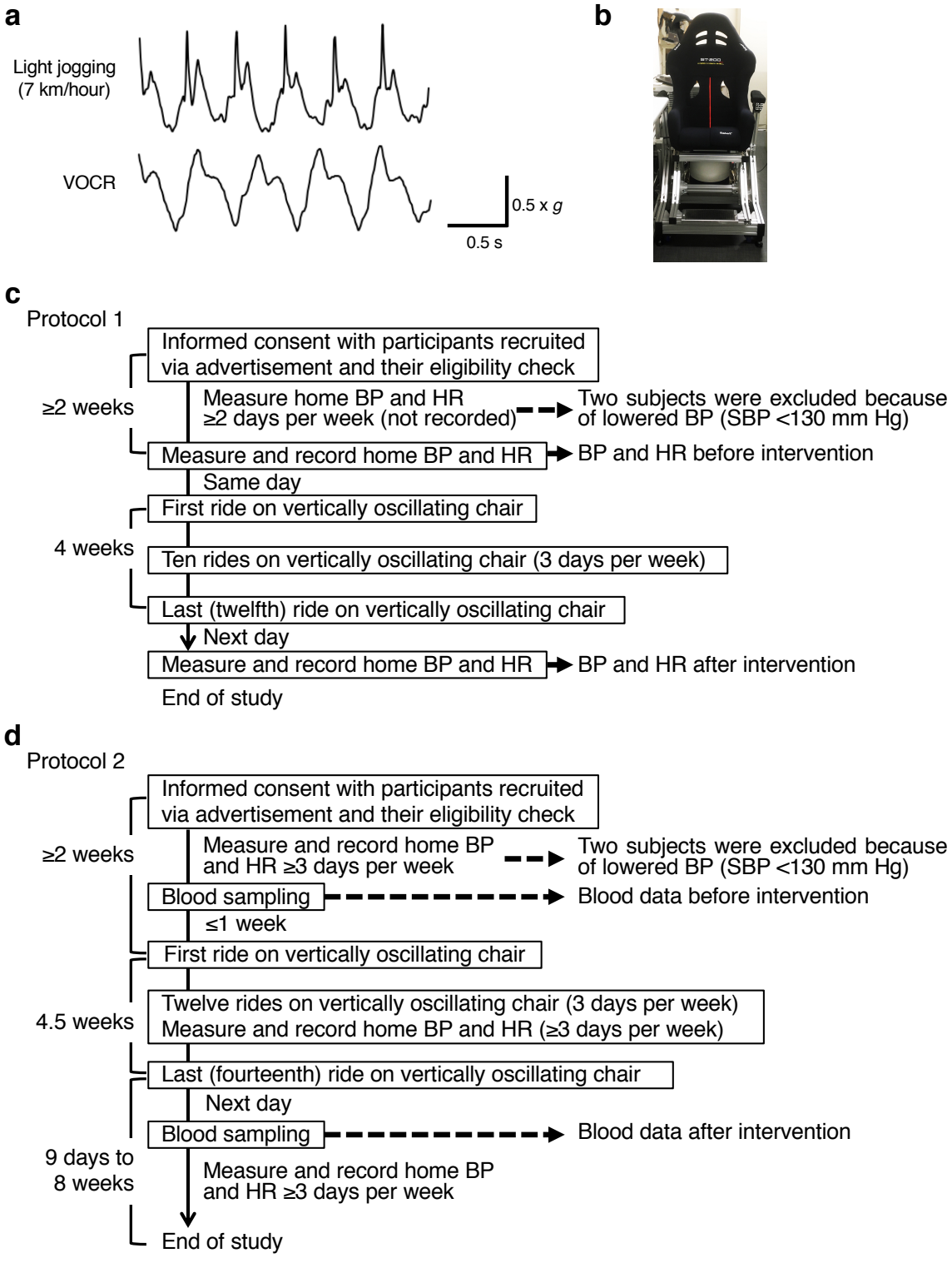

Extended Data Fig. 5 | Vertically oscillating chair that reproduces mechanical impacts on the

827 **head during light jogging, and protocols of clinical study to examine antihypertensive effect of**

828 **VOCR on hypertensive adult humans. a,** Vertical accelerations generated at adult human head

829 during light jogging on a treadmill machine (velocity: 7 km/hour) and VOCR (frequency: 2 Hz).

830 The VOCR system was adjusted to produce ~1.0 x *g* vertical acceleration peaks. Right-angled scale

831 bar, 0.5 x *g* / 0.5 s. Images are representative of three independent experiments with similar results.

832 **b**, Photograph of the chair. **c,d,** Protocol 1 **(c)** and 2 **(d)**.

Extended Data Fig. 6

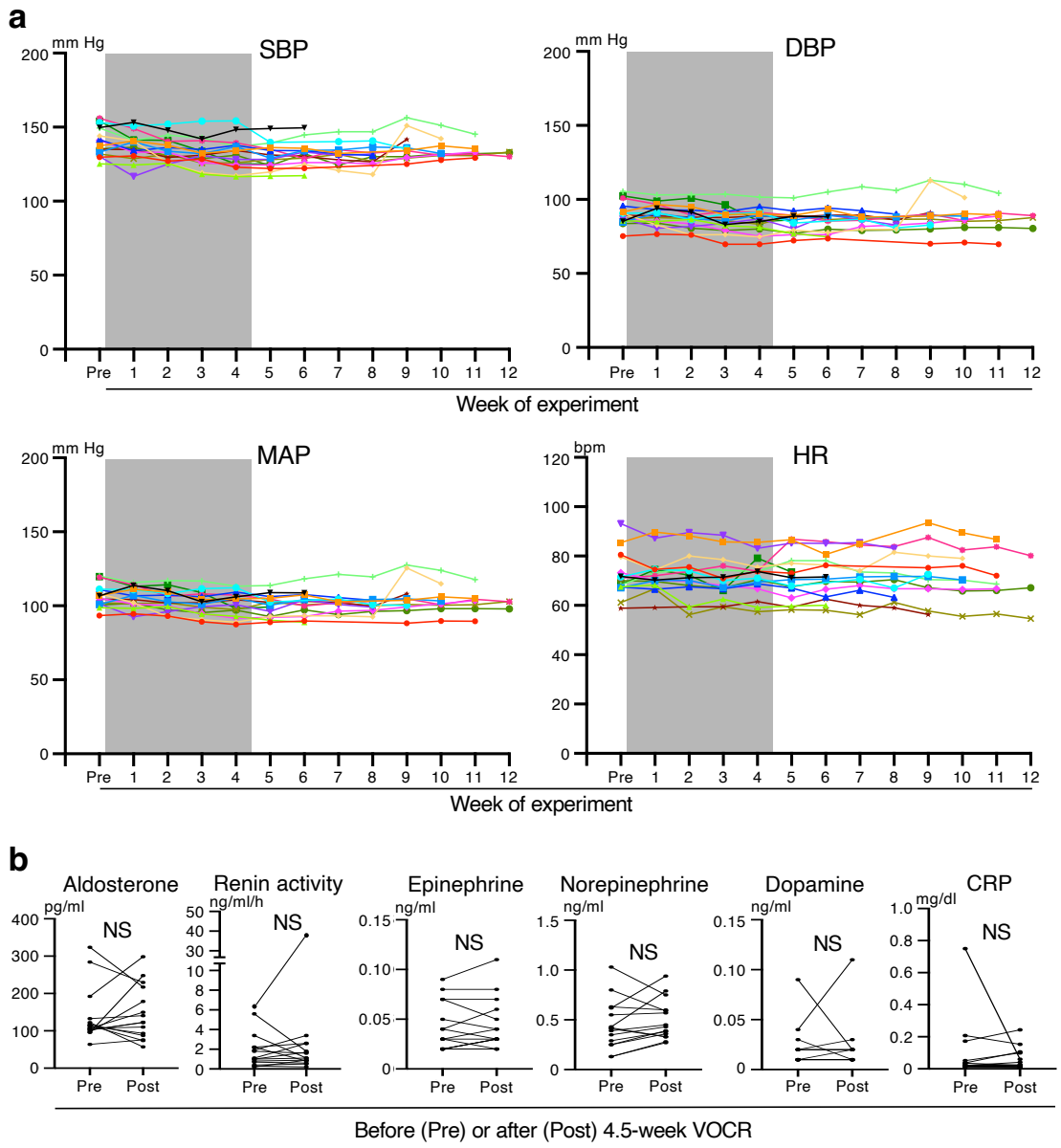

Extended Data Fig. 6 | Trajectories of BP and HR, and blood test values before and after the intervention period in the study of protocol 2. a, Trajectories of "value of the week"s of BP and HR. Gray-shaded rectangles indicate the VOCR intervention periods. The colors and symbols of individual lines correspond to those of individual subjects (Fig. 7c). The black line with inverted triangles indicates subject 9. **b,** Blood test values before and after the intervention period.

839 Significant change was not observed in any of tested parameters. NS, not significant; paired two-
840 tailed Student's *t*-test. (Aldosterone: $P = 0.6265$. Renin activity: $P = 0.3794$. Epinephrine: $P =$
841 0.5103. Norepinephrine: $P = 0.2653$. Dopamine: $P > 0.9999$. CRP: $P = 0.4412$.). A participant
842 (subject 18) showed a large increase in plasma renin activity after VOCR. We advised him to
843 consult his primary care physician, who ruled out the disqualifying conditions for this study (e.g.,
844 severe renal disease; see Methods) based on comprehensive evaluation. Therefore, we did not
845 exclude subject 18 from our statistical analysis of BP and HR.

Supplementary Table 2

Subject #	Sex / Age (years) / Body weight (kg) / Height (cm) / BMI	Period since diagnosis or self-recognition as hypertension / Health problems and diseases other than hypertension	Smoking / Alcohol (if yes, how often)	Current medication (dose per day)	Habitual exercise (times per week)	SBP/DBP (mm Hg) and HR (bpm) just before (left) and after (right) VOCR period (month of first - last bout of VOCR)
1	Male 60 73 165.2 27.2	13 years Hyperuricemia	No Almost every day	Azilsartan · Amlodin (20 mg • 5 mg) Febuxostat (10 mg) Bisoprolol fumarate (5 mg)	Walking 90 minutes (3 or 4 times)	148/85 139/78 62 66 February - March
2	Female 53 50 159 19.8	14 years None	No Almost every day	None	Sit-ups 2 x 30 times (every day)	135/90 127/81 70 69 March
3	Male 37 113 186 32.7	19 years None	No Occasionally	None	Judo (once)	135/86 129/91 68 54 March
4	Female 60 73 156 30	6 years None	No Occasionally	None	None	141/87 132/80 79 80 April - May
5	Female 52 50 148 22.8	1 year None	No Occasionally	Azilsartan (20 mg) Amlodin (2.5 mg)	None	144/84 140/80 74 69 April - May
6	Female 57 68 164 25.3	10 years None	No Occasionally	None	None	128/70 109/70 77 76 November - December
7	Male 61 67 168 23.7	Uncertain (<1 year) Diabetes mellitus Hyperlipidemia	No No	Metformin hydrochloride (1000 mg) Rosuvastatin calcium (5 mg) Sitagliptin phosphate hydrate (50 mg)	Walking 120 minutes (once)	146/100 128/86 92 84 November - December
8	Male 46 72 178 22.7	3 months Allergic rhinitis	Yes Occasionally	Montelukast sodium (10 mg) Ebastine (10 mg)	Walking 60 minutes (once) Stretching 30 minutes (once)	135/95 118/78 61 59 November - December
9	Male 55 87 173 29.1	7 months Diabetes mellitus	No No	None	Karate (2 or 3 times)	156/89 145/94 74 67 November - December
10	Male 70 62 166 22.5	6 months None	No Occasionally	None	Walking 40 minutes (4 times)	140/92 121/79 81 89 November - December
11	Female 60 45 157 18.3	Uncertain (>1year) Breast cancer (post-surgery)	No Almost every day	Tamoxifen citrate (20 mg)	None	155/92 136/81 74 67 November - December
12	Male 68 72 171 24.6	Uncertain (<1 year) None	No No	None	None	133/86 129/88 70 70 January - February
13	Female 56 58 160 22.7	7 years None	No No	Telmisartan • Amlodipine (40 mg • 5 mg)	None	137/95 133/93 65 71 January - February
14	Male 49 69 168 24.5	Uncertain (<1 year) Diabetes mellitus	No No	Sitagliptin phosphate hydrate (50 mg) Acetazolamide (250 mg)	None	140/90 124/77 95 83 January - February

Subject #	Sex Age (years) Body weight (kg) Height (cm) BMI	Period since diagnosis or self-recognition as hypertension Health problems and diseases other than hypertension	Smoking Alcohol (if yes, how often)	Current medication (dose per day)	Habitual exercise (times per week)	SBP/DBP (mm Hg) and HR (bpm) just before (left) and after (right) VOCR period (month of first - last bout of VOCR)	
15	Male 43 69 165 25.3	Uncertain (<1 year) None	No Occasionally	None	None	140/87 76 August - September	124/75 62
16	Female 48 45.3 157.2 18.3	15 years None	No Occasionally	None	Walking 60 minutes (6 times)	157/101 72 October - November	140/92 96
17	Male 65 60.1 167.1 21.5	8 years None	Yes Almost every day	None	None	140/93 59 October	134/89 56
18	Male 55 93.4 168.1 33.1	8 years Reflex esophagitis Hyperlipidemia	No Almost every day	Azilsartan (20 mg) Lansoprazole (15 mg) Atorvastatin calcium hydrate (10 mg) Benidipine hydrochloride (4 mg)	None	172/123 69 November - December	115/78 88
19	Male 41 92.3 183.2 27.5	2 years None	No Almost every day	None	Walking 60 minutes (3 times)	130/83 64 January - February	127/89 56
20	Female 65 48.7 158.6 19.4	1 year Hyperlipidemia Lumbar spinal canal stenosis (post-surgery)	No Almost every day	Amlodipine besilate (5 mg) Atorvastatin calcium hydrate (10 mg) Limaprost alfadex (15 μg) Loxoprofen sodium hydrate (120 mg) Rebamipide (200 mg)	Swimming 40 minutes (5 times)	136/87 70 January - February	118/75 67
21	Male 32 65.1 168.9 22.8	2 years None	No Almost every day	None	None	163/109 71 January - February	126/86 80

Supplementary Table 2 | Information of subjects who participated in the human studies.

Subjects 1−5 were participants in the study of protocol 1, and subjects 6−21 participated in the study of protocol 2. Subject 9 was excluded from our statistical analysis because of high serum CRP value before VOCR (2.85 mg/dL), which made it difficult to rule out acute infection, a possible disqualifier, at the time of initiation of VOCR, albeit the lack of specific complaint or local symptom related to acute physical problem(s). His serum CRP after the VOCR period was within the normal range (0.12 mg/dL).

Extended Data Fig. 7

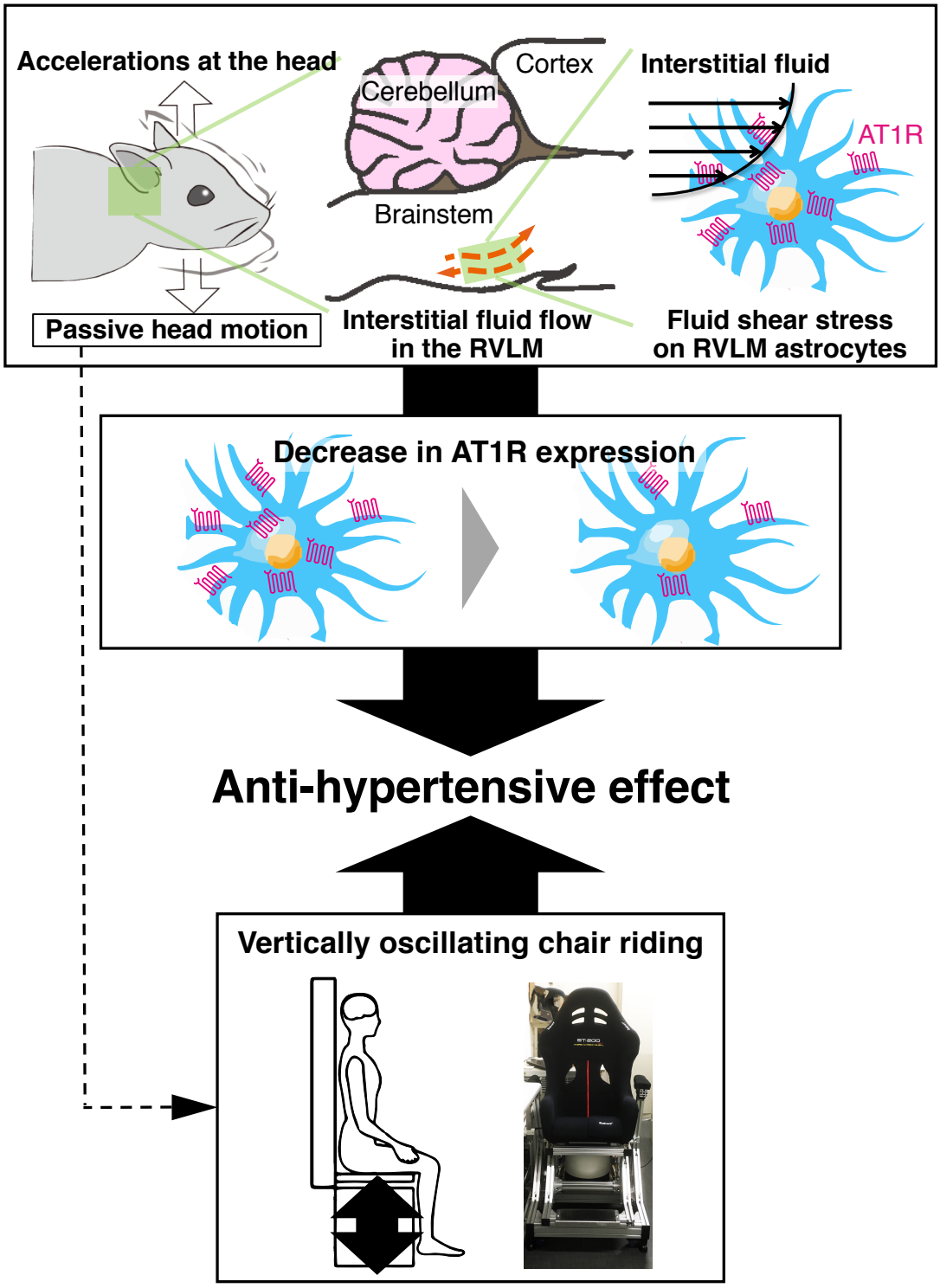

Extended Data Fig. 7 | Schematic representation of the antihypertensive effects observed in

PHM of hypertensive rats and VOCR of hypertensive humans. The results from our animal experiments indicate that cyclical mechanical impact on the head generates interstitial fluid movement in the RVLM, leading to FSS-induced decrease in AT1R expression in astrocytes in situ, and thereby ameliorates hypertension. Our studies also show that the VOCR of hypertensive adult humans, which produces vertical accelerations at their heads, lowers their BP.

Methods

Animal experiments and human studies. Animals were housed under a 12/12 hour light-dark cycle with controlled temperature (23−25°C), and treated with humane care under approval from the Animal Care and Use Committee of National Rehabilitation Center for Persons with Disabilities (approval number: 30-07). Male SHRSP/Izm and WKY/Izm rats were provided from the Disease Model Cooperative Association (Kyoto, Japan) and astrocyte-GFP mice (Aldh1L1-GFP mice)[37] were obtained from GENSAT (New York, NY), acclimated to the laboratory environments for at least 1 week, randomly divided into experimental groups, and used for experiments.

All participants in our human studies provided written informed consent. The studies were approved by the Ethics Committees of the Iwai Medical Foundation and the National Rehabilitation Center for Persons with Disabilities (approval number: 30-01).

Chemicals and antibodies. All the chemicals were purchased from Sigma-Aldrich unless noted otherwise. Primary antibodies and their dilution rates used in this study are as follows: mouse monoclonal anti-GFAP (MAB360; Millipore, Billerica, MA) at 1:1,000; rabbit polyclonal anti-GFAP (Z0334; Dako, Glostrup, Denmark) at 1:1,000; chicken polyclonal anti-GFAP (ab4674; Abcam, Cambridge, UK) at 1:2,000; rabbit polyclonal anti-cleaved caspase-3 (9661; Cell Signaling Technology, Danvers, MA) at 1:1,000; mouse monoclonal anti-NeuN (MAB377; Millipore) at

1:200; rabbit polyclonal anti-NeuN (ABN78; Millipore) at 1:1,000, rabbit polyclonal anti-AT1R (HPA003596; Sigma-Aldrich, St. Louis, MO) at 1:200; rabbit polyclonal anti-AGTRAP (HPA044120; Sigma-Aldrich) at 1:1000; rabbit polyclonal anti-GFP (598; MBL, Nagoya, Japan) at 1:2,000; chicken polyclonal anti-GFP (ab13970; Abcam) at 1:2,000; mouse monoclonal anti-TUJ-1 (ab78078; Abcam) at 1:1000. Secondary antibodies conjugated with Alexa Fluor 350, 488, 568, 633, and 647 (Thermo Fisher Scientific, Waltham, MA) were used at the dilution rate of 1:400. Cell nuclei were stained with DAPI (D9542; Sigma-Aldrich).

PHM application to rats. Rats were subjected to PHM in a prone position using a platform that we developed to move their heads up and down[24] (schematically represented in Fig. 1a). During PHM, animals were kept anesthetized with 1.5% isoflurane except for the μCT study, in which we used intraperitoneal injection of 2 mg/kg of midazolam (Sandoz, Basel, Switzerland), 2.5 mg/kg of butorphanol (Meiji Seika, Tokyo, Japan) and 0.15 mg/kg of medetomidine (Kyoritsu Seiyaku, Tokyo, Japan) for anesthesia. Body temperature of tested animals was maintained using a light heater. The PHM system was set up to reproduce the head motion (5 mm, 2 Hz) of treadmill running (20 m/minute) which made 1.0 x *g* vertical acceleration peaks at the head of rats examined[24]. The control rats in PHM experiments were anesthetized likewise, and placed in a prone position with their heads on the platform that was left static.

Treadmill running of rats. Rats were subjected to compulsive running using a belt drive treadmill equipped with an electrical shock system (MK-680S; Muromachi, Tokyo, Japan). We habituated the rats to the treadmill system by placing them in the machine several times without turning on the treadmill belt during the acclimation period. The electrical stimulation was turned on only once or twice during the first 5 minutes of the 30-minute treadmill running on the first day of the 4-week treadmill running period. Thereafter, we did not need to turn on the electrical shock system to have the animals keep running, perhaps because the velocities we employed (20 m/minute) were moderate. The control rats in treadmill running experiments were placed on the belt daily for 30 minutes without turning on the treadmilling.

Measurement of BP and HR of rats by radio-telemetry. Rats were implanted with a telemetry pressure probe (Millar, Houston, TX) in the abdominal aorta at 9−10 weeks of age, following the surgical procedure described previously[61]. Rats were allowed to recover for at least 14 days before the initiation of experimental interventions or analyses. During the periods of experimentation that involved repeated BP and HR measurements over multiple weeks, BP and HR were monitored and recorded for continuous 30 minutes every 7 days between 10:00 AM and 12:00 PM (noon) by a multichannel amplifier and signal converter (LabChart 8; ADInstruments, Dunedin, New Zealand).

Mean arterial pressure (MAP) was calculated with a standard formula as follows: MAP = diastolic BP (DBP) + 1/3 [systolic BP (SBP) – DBP].

Measurement of urinary norepinephrine excretion of rats. Urine excreted during the indicated 24-hour period was collected by means of a metabolic cage (KN-646; Natsume Seisakusho, Tokyo, Japan), and stored at −80˚C until assayed. Excretion of urinary norepinephrine was calculated by multiplying its concentration measured using an enzyme-linked immunosorbent assay (ELISA) kit (KA1891; Abnova, Taipei, Taiwan) with the urine volume.

Microinjection into rat RVLM. Rats were anesthetized with intraperitoneal injection of midazolam, butorphanol, and medetomidine except for Ang II or valsartan injection studies, in which we used 1.2−1.4 g/kg of urethane (Sigma-Aldrich), and subjected to microinjection as described previously[62]. In brief, a 25s-G microsyringe (Hamilton, Bonaduz, Switzerland) was stereotaxically positioned on anesthetized rats after exposure of dorsal surface of medulla. The needle placement was defined according to an atlas of the rat with stereotaxic coordinates[63]; anteroposterior angle: 18˚, 1.8 mm lateral to the calamus scriptorius, 3.5 mm ventral to the dorsal surface of the medulla. The placement of the needle tip in RVLM was confirmed by ensuring the pressure response to a test-dose injection of L-glutamate[12,64] (100 nL of 1 mmol/L in PBS).

936 Microinjection of various compounds or mediums was made through a needle reinserted at the
937 same coordinates with fixed infusion rates using a microsyringe pump instrument (KD scientific,
938 Holliston, MA). Except for experiments to analyze pressor or depressor responses, we held the
939 syringe for 5 minutes after the injection to avoid reflux, pulled out the needle carefully, and sutured
940 the skin. The volumes and rates of microinjection were as follows; Ang II (Auspep, Tullamarine,
941 Australia) and valsartan (Tocris Bioscience, Bristol, UK): 100 nL of 1 mmol/L in PBS at 0.1
942 μL/minute, AAV solutions: 300 nL at 0.03 μL/minute, PEG solutions: 1 μL at 0.1 μL/minute,
943 Isovist: 1 μL at 0.2 μL/minute.
944
945 **Analysis of pressor/depressor responses.** Rats implanted with a telemetry pressure probe were
946 anesthetized with urethane, and subjected to the analysis of pressor/depressor responses. Monitoring
947 the BP, we injected Ang II or valsartan (100 pmol) stereotaxically into the unilateral RVLM
948 following the microinjection procedures described above. The injection side (right or left) was
949 chosen randomly. When both pressor and depressor responses were analyzed, at least 2 hours
950 elapsed between the injections of Ang II and valsartan (Fig. 2a). The maximal MAP change elicited
951 from the baseline was statistically analyzed[14].
952
953 **Production of AAV vectors.** To obtain astrocyte- and neuron-specific transduction, we used AAV9

vectors that expressed a transgene under the control of mouse GFAP and rat NSE promoters, respectively. The astrocyte-specific GFAP promoter consists of 0.6-kb hybrid fragments containing ABC1D genomic regions upstream of the mouse *GFAP* gene[65]. The neuron-specific NSE promoter is composed of the 1.2-kb genomic region upstream of the rat *NSE* gene[66]. Full-length rat AGTRAP cDNA was synthesized (Eurofins Genomics, Tokyo, Japan) and inserted into plasmid pAAV-GFAP-GFP-P2A-Cre-woodchuck hepatitis virus post-transcriptional regulatory element (WPRE)-simian virus 40 polyadenylation signal (SV40pA) and pAAV-NSE-GFP-P2A-Cre-WPRE-SV40pA to generate pAAV-GFAP-GFP-P2A-AGTRAP-WPRE-SV40pA and pAAV-NSE-GFP-P2A-AGTRAP-WPRE-SV40pA. pAAV-GFAP-GFP-WPRE-SV40pA and pAAV-NSE-GFP-WPRE-SV40pA were used for experimental controls. Recombinant single-strand AAV2/9 vectors were produced by transfection of HEK293T cells (Thermo Fisher Scientific) with the respective pAAV expression plasmid, pAAV2/9 and a helper plasmid (Stratagene, La Jolla, CA) as previously described[67]. After harvesting conditioned medium, the viral particles were precipitated using polyethylene glycol 8000 and iodixanol continuous gradient centrifugation as previously described[68]. The genomic titer of purified AAV9 vectors was determined by qPCR that targeted the WPRE sequence.

Measurement of pressure in rat RVLM. Intra-brainstem pressure (IBP) was measured using a

blood pressure telemeter by means of the procedure we previously reported[24,69]. The pressure sensor was placed in rat RVLM using the same approach with the microinjection described above. During IBP measurement, respiration was monitored using a respiration sensor attached to the tested rats. Low-pass (50 Hz) filtered IBP waves were analyzed using LabChart 8 software (ADInstruments). We observed ~0.5-Hz respiration-synchronized IBP changes with ~2.5 mm Hg magnitude (peak to peak) as well as 2-Hz PHM-specific waves with ~1.2 mm Hg magnitude (peak to peak).

In vivo analysis of the distribution dynamics of interstitial fluid in rat RVLM using μCT. Isovist (Bayer, Berlin, Germany) was stereotaxically microinjected into RVLM of anesthetized 12-week-old male WKY rats following the procedure described above, and visualized using μCT (inspeXio SMX-100CT, Shimadzu, Kyoto, Japan). After Isovist injection, rats were subjected to two serial brain μCT scans between which PHM was either applied or left unapplied (kept sedentary) for 30 minutes (Fig. 4e). μCT images were analyzed using software for 3D morphometry (TRI/3D-BON-FCS64, RATOC System, Tokyo, Japan). Voxels with ≥1.02 times signal intensity as compared with that of air was defined as Isovist cluster in rat RVLM.

Simulative calculation of the magnitude of FSS on the cells in rat RVLM during PHM. We calculated interstitial fluid flow-derived FSS imposed on cells in rat RVLM by referring the results

990 from our μCT analysis (Fig. 4g,h) to the Henry Darcy's law, which defines the flux density of
991 penetrating fluid per unit time[70]). The velocity of interstitial fluid flow (u) is assumed to approach
992 the superficial velocity (u_∞) and zero (u=0) at the cell surface (i.e., a no-slip condition). Using these
993 two boundary conditions together with the Brinkman equation, FSS (τ) at the interstitial cell surface
994 can be obtained as described in Supplementary Table 1[60].
995
996 **Cell culture.** Primary cultures of astrocytes were prepared from the cortex of neonatal (2−3 days
997 old) astrocyte-GFP mouse[37] pups by physical dissociation as previously described[71]. Cells were
998 maintained in DMEM/F12 supplemented with 10% FBS (GE Healthcare Life Science,
999 Marlborough, MA), 100 I. U./mL penicillin and 100 μg/mL streptomycin at 37°C in a humidified
1000 incubator (5% CO_2 and 95% air). Culture medium was replaced with fresh one every 3−4 days until
1001 confluent. Astrocytes were detached with trypsin/EDTA (0.05% trypsin, 0.53 mM EDTA in PBS),
1002 replated at a ratio of 1:10, and grown to approximately 80−90% confluence prior to use.
1003 Mouse neuroblastoma-derived Neuro2A cells (provided from Dr. Yokota, Tokyo Medical and
1004 Dental University, Japan), which exhibit neuronal phenotypes and morphology[39,40], were cultured in
1005 DMEM (Wako, Japan) supplemented with 10% FBS, 100 I. U./mL penicillin and 100 μg/mL
1006 streptomycin at 37°C in a 5% CO_2 incubator.
1007

Application of FSS to astrocytes or Neuro2A cells in culture. Astrocytes or Neuro2A cells grown in a poly-D-lysine-coated 35-mm culture dish (Corning Life Sciences, Corning, NY) were exposed to pulsatile FSS (average 0.7 Pa) for 30 minutes. As we previously reported[23,24,35], a parallel plate flow-chamber and a roller pump (Masterflex; Cole-Parmer, Vernon Hills, IL) were used to apply FSS. The flow-chamber, which was composed of a cell culture dish, a polycarbonate I/O unit, and a silicone gasket, generated a 23-mm-long 10-mm-wide 0.5-mm-high flow channel. To maintain pH and temperature of culture medium, we used a 5% CO_2-containing reservoir and a temperature-controlled bath.

Tissue preparation and immunostaining (immunohistochemical or immunocytochemical analysis). Rats were anesthetized with intraperitoneal injection of midazolam, butorphanol, and medetomidine, and perfused transcardially with 4% paraformaldehyde (PFA; TAAB Laboratories Equipment, Aldermaston, UK). The brainstems were excised and post-fixed with 4% PFA in PBS overnight at 4°C. The tissues were cryoprotected by soaking in 20% sucrose/PBS for 24 hours and in 30% sucrose/PBS for additional 24 hours at 4°C. Fixed brainstems were frozen in optimal cutting temperature (OCT) compound (Sakura Finetek, Tokyo, Japan) and cut into 16 μm-thick coronal sections using a cryostat (CM3050S; Leica Microsystems, Wetzlar, Germany). Sliced sections were permeabilized and blocked with 0.1% Tween-20 and 4% donkey serum (Merck Millipore,

Burlington, MA) in Tris-buffered saline, blocked with, and stained by incubating with primary antibodies at appropriate dilutions followed by their species-matched secondary antibodies. Cell nuclei were stained with DAPI (Sigma-Aldrich). The slides were mounted with ProLong Gold Antifade Reagent (Thermo Fisher Scientific) and images were captured with a BZ-9000 digital microscope system (Keyence, Osaka, Japan).

For immunocytochemistry, cultured cells were fixed with 4% PFA in PBS for 20 minutes at room temperature (RT) and permeabilized and blocked with 0.1% Triton X-100 and 10% FBS (Thermo Fisher Scientific) in PBS for 30 minutes at RT. The cells were then incubated with primary antibodies for 2 hours and then with secondary antibodies for 1 hour at RT.

Quantitative PCR Analysis (reverse transcription and real-time PCR). 500 ng of total RNA extracted from cell culture were subjected to reverse transcription, using ISOGEN II (NIPPON GENE, Tokyo, Japan) and PrimeScript RT reagent Kit (TaKaRa, Kusatsu, Japan). The resulting cDNA was subjected to real-time PCR analysis using glyceraldehyde-3-phosphate dehydrogenase (GAPDH) as an internal control in Applied Biosystems 7500 Real Time PCR System with Power SYBR Green PCR Master Mix (Thermo Fisher Scientific).

The primers (sense and antisense, respectively) were as follows: mouse *Agtr1a* (AT1R-encoding gene); 5'-AAAGGCCAAGTCGCACTCAAG-3'

and 5’-TCCACCTCAGAACAAGACGCA-3’,

mouse *Gapdh* (GAPDH-encoding gene); 5’-GCAAAGTGGAGATTGTTGCCAT-3’ and

5’-CCTTGACTGTGCCGTTGAATTT-3’, WPRE (for genomic titration of purified AAV9 vectors);

5’-CTGTTGGGCACTGACAATTC-3’ and 5’-GAAGGGACGTAGCAGAAGGA-3’.

Fluorescent Ang II binding assay. Six or twenty-four hours after the termination of FSS application, cultured astrocytes were incubated with Ang II type 2 receptor inhibitor, PD123319 (10^{-6} mol/L in PBS; ab144564, Abcam), for 20 minutes, and then with tetramethylrhodamine (TAMRA)-labeled Ang II (10^{-8} mol/L in PBS; AS-61181, AnaSpec, Fremont, CA) for 30 minutes. After 3 times wash with PBS, samples were fixed and subjected to anti-GFP immunostaining to strengthen the GFP-derived green fluorescence signals and corroborate our analysis on astrocytes prepared from astrocyte-GFP mice as well as to secure the binding of fluorescent Ang II. Green and red fluorescence was viewed with a fluorescence microscope (BZ-9000 HS, Keyence). Samples from astrocytes left unexposed to FSS were prepared and viewed likewise, and provided an experimental control.

Hindrance of interstitial fluid movement (flow) by introduction of hydrogel in rat RVLM. Just before use, a pre-mixture of polyethylene glycol (PEG) with functional groups (25 g/L in PBS) was

prepared from tetra-armed thiol-terminal (TetraPEG-SH) (Yuka-Sangyo, Tokyo, Japan) and acrylate-terminal (Tetra-PEG-ACR) (JenKem Technology, TX, USA) PEG solutions as we previously described[24]. Tetra-armed polyethylene glycol without functional groups (25 g/L in PBS) was used as an ungelatable control. For the analysis of hydrogel distribution in rat RVLM, we used Tetra-PEG-SH fluorescently labeled with a thiol-reactive probe (Merck KGaA, Darmstadt, Germany). Microinjection of PEG solutions into rat RVLM was conducted as described above.

To specifically analyze the consequences of PHM and hydrogel introduction by minimizing possible invasive influences of microinjection itself, we gave 1-week recovery time before the first BP measurement, and then applied PHM to the rats (daily 30 minutes, 14 or 28 days). Immediately subsequent to post-PHM 24-hour urine collection (Fig. 6a), rats were sacrificed by transcardial infusion of PFA and subjected to histological analysis.

Terminal deoxynucleotidyl transferase-mediated dUTP nick-end labeling (TUNEL) assay. Rat RVLM sections were stained using a TUNEL kit (Biotium, Fremont, CA) according to the manufacturer's protocols, counterstained with DAPI, and then viewed using a 20x objective with a fluorescence microscope (BZ-9000 HS, Keyence). The nuclei of apoptotic cells were determined by the existence of green fluorescent patches, and cell apoptosis was quantified by referring their counts to total numbers of nuclei defined by DAPI staining.

Measurement of accelerations at human head. To measure the accelerations at the human head during treadmill running or VOCR, we fixed an accelerometer (NinjaScan-Light; Switchscience, Tokyo, Japan) on foreheads with a surgical tape. Vertical acceleration was evaluated using the software application provided from the manufacture.

Blood sampling and measurement of parameters in plasma and serum of humans. Blood sampling in the human study of protocol 2 was conducted between 12 PM and 3 PM. Participants were rested in a sitting position for at least 10 minutes before starting the sampling procedures. After plasma (for catecolamines and renin activity) and serum (for aldosterone and CRP) separation by centrifugation, we outsourced the measurement of parameters be tested (BML, Kawagoe, Japan).

Design and participants of clinical study on antihypertensive effects of vertically oscillating chair riding. We conducted single-arm clinical studies. The study of protocol 1 (Extended Data Fig. 5c) was carried out at the affiliated health services facility of Iwai Medical Foundation (Iwai Keiaien, Tokyo, Japan). The study of protocol 2 (Extended Data Fig. 5d) was carried out at the National Rehabilitation Center for Persons with Disabilities Hospital.

Subjects were considered eligible if they were 20−75 years old of age and confirmed to have

130−160 mm Hg of SBP at the time of interview for informed consent and eligibility check. Subjects with mental or psychological illnesses, history or presence of cardiovascular events, history or presence of severe dysfunction/disorder of liver, kidney, lung, gastrointestinal tract, and spine, or presence of acute injuries/diseases (e.g., recent traumas and infectious diseases) were excluded with the exception of those who were given permission for participating in this study from their primary care physicians. Whereas antihypertensive medication did not disqualify the subjects (Supplementary Table 2), they were advised not to change their medication from at least one month prior to the first bout of VOCR through the study period (i.e., up to 8 weeks after the last bout of VOCR). At a certain (approximately fixed) time point in the morning (typically just before breakfast), they conducted 3 consecutive measurements of BP (mm Hg) and HR (bpm) using an automated upper arm-cuff sphygmomanometer, and recorded the values from all those measurements. These procedures of BP measurement and recording accord with the Japanese Society of Hypertension Guidelines for the management of hypertension (JSH2019)[72]. Subjects were directed to start periodical (≥3 days per week) BP/HR measurements at least 2 weeks before the initiation of the intervention (i.e., daily VOCR) and continue to measure BP/HR throughout the study period using the same sphygmomanometers. Particularly at the study of protocol 2 (i.e., the study at the National Rehabilitation Center for Persons with Disabilities), participants were advised to record all the data of those measurements. Those whose BP lowered below the eligibility

requirement of the study (≥130 mm Hg of SBP) prior to the initiation of VOCR intervention were eliminated from the study. Participants were directed to be rested and keep calm for at least 1 minute before starting to measure BP/HR. The mean BP/HR value from 3-time measurements was defined as "value of the day", and used for statistical analysis. When BP and HR were measured and recorded on ≥3 days during a particular week in the study of protocol 2, the mean of all the "value of the day"s through the week was defined as "value of the week". For the participants who agreed. periodical BP/HR measurement and recording (≥3 days per week) was extended up to 8 weeks after the last bout of VOCR.

Statistical analysis. All the quantitative data are presented as mean ± s.e.m. Parametric statistical analyses were conducted by paired or unpaired two-tailed Student's *t*-test for two-group comparison, and ANOVA with Tukey's post hoc test for multiple (≥3) group comparison, using Prism software (Version 8, GraphPad Software, San Diego, CA). Differences were considered as significant at *P* values below 0.05.